Application of the Snowmelt Runoff Model to Projecting Climate Change Impacts on Flow in the Upper Athabasca River Basin

By

Kyle Alexander Siemens

B.Sc. University of Victoria, 2014

A Thesis Submitted in Partial Fulfillment of the

Requirements for the Degree of

MASTER OF SCIENCE

in the Department of Geography

Supervisory Committee

Application of the Snowmelt Runoff Model to Projecting Climate Change Impacts on Flow in the Upper Athabasca River Basin

By

Kyle Alexander Siemens
B.Sc. University of Victoria, 2014

Supervisory Committee

Dr. Terry D. Prowse (Department of Geography)

Supervisor

Dr. Yonas B. Dibike (Department of Geography)

Departmental Member

Abstract

Supervisory Committee

Dr. Terry D. Prowse (Department of Geography)

Supervisor

Dr. Yonas B. Dibike (Department of Geography)

Departmental Member

The projected rise in global temperatures will shift runoff patterns of snowmelt dominated basins, resulting in earlier spring peak flows and reduced summer runoff. Projections of future runoff are beneficial in preparing for climate change induced changes in streamflow, which may necessitate the construction of additional artificial reservoirs to compensate for the reduced natural storage in the form of snow. In this study, the Snowmelt Runoff Model (SRM) was applied to projecting future runoff in the Upper Athabasca River after assessing its ability to simulate historical flows in the basin. SRM utilizes the data-light degree day approach to modelling snowmelt, assuming melt to be proportional to the temperature above freezing through the degree day factor (DDF). Nevertheless, the model performed very well in simulating flows over both the calibration (2000-2002) and validation (2003-2010) periods. The inclusion of a separate DDF for glaciated areas was found to be essential in accurately simulating over multiple years with varying snow conditions. The increased melt rate of glacial ice due to its lower albedo relative to snow could explain most of the elevation dependence of the DDF. The SRM with glacier component was applied with four future (2070-2080) climate change scenarios representing uncertainty in climate change projections over the basin. The results show a consistent pattern of change in runoff across all scenarios, with substantial

increases in May runoff, minor increases over the winter months, and decreased runoff in summer months (June-August). Projected flows are consistent with past modelling studies for the region and with historical trends. In general, the SRM performed very well in simulating historical flows and provides useful runoff projections despite the relative simplicity and few input variables of the model.

Table of Contents

List of Figures

List of Tables

1 Chapter 1: Introduction

1.1 Background

Water resources have been vital to human populations throughout history, utilized for drinking water, irrigation of crops, hydropower production, and industrial use. Despite its abundance on the earths surface, the availability of fresh water is spatially and temporally variable. Many populations in arid and semi-arid regions rely on runoff originating from nearby humid mountainous regions for their water supply (Shen and Chen, 2010). For most regions north of 45°N and at high elevation at lower latitudes, this runoff is dominated by snowmelt (Barnett et al., 2005). The winter snowpack acts as a natural reservoir, storing winter precipitation and releasing it over the spring and summer. With the seasonal distribution of runoff largely governed by temperature in snowmelt dominated regions (Adam et al., 2009), a warming climate will reduce this natural storage capacity, resulting in earlier peak flows in spring and lower flow in summer. This shift is problematic given water use for irrigation and municipal water withdrawals peaks in summer (Schindler and Donahue, 2006). Regions which rely on a deep winter snowpack to maintain summer water supplies may have to construct artificial reservoirs to compensate for this loss of natural storage.

The Canadian Prairies are one such semi-arid landscape, reliant on surface runoff and ground water originating from the snowmelt dominated Canadian Rocky Mountains. Water withdrawal on the Canadian Prairies primarily utilizes surface water, unlike the Great Plains of the United States which extensively exploit groundwater (Gan, 2000). Nearly 50% of water withdrawals on the Prairies have historically been used for irrigation (Gan, 2000). Water is also withdrawn for

municipal and industrial use, with the oil sands industry on the Athabasca River being a notable consumer. Observed streamflow data shows the shift towards earlier spring freshet, and lower summer flows have been occurring throughout the Rocky Mountains over the past century (Rood et al., 2008, Bawden et al., 2014) corresponding to observed increases in temperature (O'Neil et al., 2016a). Climate models project continued warming for the region, with a 1.5-2.5°C increase in average daily maximum and a 3°C increase in average daily minimum temperatures for 2041-2070 relative to 1971-2000 (O'Neil et al., 2016b).

Modelling runoff provides useful information on the future availability of water which can be used in the management of water resources. Modelling runoff in basins where snow is present requires quantifying the accumulation and depletion of the snowpack. Hydrological models take different approaches to handling these processes. Two of the common approaches utilized in quantifying snowmelt are the energy balance and degree-day methods. While the physically based energy balance approach provides a more accurate calculation of melt given all the necessary data, the relatively high data requirements with very limited observed data often results in estimating most model inputs (Day, 2009). Wherever observed data is sparse, the error introduced from interpolating meteorological variables to the site of interest nullifies the accuracy advantage of using an energy balance model in the first place. In contrast, the degree day method requires only temperature as an input, taking advantage of the high correlation between melt and air temperature (Hock, 2003). Temperature is relatively easy to observe and interpolate, and the simplicity of the degree day method makes it a common choice in many hydrological models (e.g. HBV, SRM, UBC). In addition to the rate of melt, hydrological models must quantify the amount of snow available for melt. This is commonly done through modelling

the accumulation of the snowpack using meteorological variables (Hock, 2005); however, the Snowmelt Runoff Model (SRM) achieves this by using satellite imagery of snow cover. Given the challenges of interpolating meteorological variables such as precipitation and modelling snow redistribution, the use of snow cover imagery is advantageous in reducing error in snow cover area. SRM uses the degree day method of calculating snowmelt, resulting in a simplistic but versatile model built on three input variables which are widely available (temperature, precipitation, remote sensed snow-cover). Therefore, the study reported in this thesis utilizes SRM to model the historical and future runoff in the Upper Athabasca River.

1.2 Thesis Objectives

The primary objectives of this thesis are to:

(1) Assess the ability of the Snowmelt Runoff Model to accurately capture runoff for the Upper Athabasca River

(2) Utilize SRM in assessing the effects of climate change on the seasonal distribution of runoff for the Upper Athabasca River

1.3 Thesis Structure

Chapter 1 provides an introduction to this thesis. Chapter 2 provides a literature review of the history of modelling snowmelt runoff, including both physically-based modelling of the energy balance of the snowpack and the development of empirical degree day models as a simplified calculation of melt. Chapters 3 and 4 are stand alone manuscripts utilizing the Snowmelt Runoff Model (SRM) to simulate discharge in the Upper Athabasca River Basin. Chapter 3 presents the calibration and validation of the model using historical data (2000-2010), while Chapter 4 applies the model to simulating future runoff in the basin for multiple climate change scenarios.

As these chapters are formatted as manuscripts, there may be some repetition in material between chapters. Chapter 5 summarizes the results of this study and provides recommendations for future research.

2 Chapter 2: Literature Review

2.1 Introduction

This chapter will provide an overview on snowpack development and melt processes including the development of energy balance modelling. It will also describe the development of the degree-day method as an alternative to energy balance models, leading into the development of Snowmelt Runoff Model (SRM) and the incorporation of remote sensing into snowmelt modelling. SRM was developed specifically for snowmelt dominated basins, and its development follows directly from early research correlating temperature with runoff. The chapter concludes with an assessment of the reported advantages and disadvantages of SRM.

2.2 Snow in the Hydrological System

In cold regions, the winter snowpack acts as a natural reservoir, storing precipitation through the winter and releasing it during the warmer months. There is a general trend towards increasing snowfall and duration of snow cover with increasing latitude and elevation, and snow cover may persist year-round at higher elevations. High altitudes may also experience tundra conditions which grade into coniferous forest at lower elevations. Snow cover may be highly unevenly distributed due to winds and slides. The redistribution of snow by winds and the spatially heterogenous rate of snowmelt caused by topography results in substantial variability in the spatial distribution and duration of snow cover.

Freshly fallen snow averages around 10% of the density of water in sub-humid environments, and around 8.3% in cold, dry environments. Once fallen, snow quickly undergoes a metamorphism which reduces snow crystal surface area, and the snow increases in density to 14-16% that of water (Bruce and Clark, 1966). Several processes contribute to compacting the

snow and creating a coarser structure, including settling due to gravity and compaction from wind. Until the snowpack becomes isothermal (at the melting point throughout its depth), melt at the snow surface will refreeze within the snowpack. This refreezing of water within the snowpack will increase the size of ice crystals and release latent heat, contributing to the compaction and warming of the snow. Rain on snow events also contribute heat both directly through the heat content of the rain and through the latent heat release from freezing within the snow. This metamorphism is associated with an increase in strength of the bonds between ice grains. Repeated freeze-thaw cycles combined with fresh snowfalls results in a complicated snow structure with numerous ice layers.

Energy input into the snowpack will raise the temperature of the snow. Once the snowpack is ripe (isothermal), additional energy input produces meltwater which is released into the ground. The energy input into the snow includes incoming and reflected shortwave radiation, incoming and emitted longwave radiation, sensible and latent heat fluxes, heat flux from rain, and conduction from the ground below the snowpack. Energy balance models quantify all these energy fluxes for melt calculations (see Eqn. 1). Incoming shortwave (solar) radiation varies temporally with season and time of day, as well as spatially with latitude and local topography. Reflected solar radiation (outgoing shortwave) varies with the albedo of the material, with fresh snow reflecting up to 90% of incident radiation. Incoming longwave radiation primarily originates from the atmosphere and can be approximated using air temperature and pressure. Snow emits radiation (outgoing longwave) in accordance with its temperature. The sensible heat flux refers to conduction between the snow surface and the atmosphere, and is proportional to the temperature gradient between the two. Similarly, the latent heat flux

results from a vapor pressure gradient, with a positive vapour pressure gradient resulting in condensation and energy release, while a negative vapour pressure gradient will result in energy loss to evaporation. Rain falling and freezing on snow will release latent heat, thereby warming the snowpack. If the rain does not freeze, the energy released into the snowpack will be equal to the difference between the initial energy in the water droplet and its energy after coming to thermal equilibrium within the snow. Finally, the energy transfer due to conduction from the ground at the base of the snowpack is proportional to the temperature gradient at the snow base.

Melt water movement from the snow surface to the ground can be slow, ranging from two to sixty centimetres per minute (Gray and Male, 1981). While initially ice layers in the snow inhibit the vertical drainage of water, within a few hours drainage channels develop allowing water to quickly travel vertically through these ice layers. Upon reaching the snowpack base meltwater will percolate into the ground or flow along the surface once the ground becomes saturated. The time taken for meltwater to percolate through the snowpack, move downhill as sub-surface or surface flow to a stream, and flow through the stream to the point of interest, all contribute to the total lag time between the time of melt and the time water appears at a gauging location.

2.3 Modelling Approaches

2.3.1 Energy Balance Models

For the many regions of the world where runoff is dominated by snowmelt, it is important to accurately quantify the amount and timing of snowmelt for flood prediction and water-

resource management. Melt models can be divided into two primary types: energy-balance models and degree-day models, with a gradient of intermediary forms in between. Energy-balance models seek to evaluate the various fluxes contributing to melt for a more physically based computation of melt, while degree-day models utilize only temperature. Despite their simplicity, degree-day models can provide an accurate calculation of melt in locations which may lack the data required for the energy balance method.

Ahlmann (1935) derived the first empirical formula for the computation of ablation in the 1920s using incident radiation, air temperature, and wind velocity (Hock, 2005). Svedrup (1935) studied ablation on Isachsen's Plateau, performing an energy balance to determine the relative contributions of energy balance components to ablation. For the period of June 26th to August 15th, the total ablation was calculated to be 42.5 cm, compared to the measured ablation of 41.5 cm. It was calculated that radiation caused 56% of the total ablation, conduction from the air caused 29.4%, and condensation of water vapor caused 14.7%. Evaporation caused 3.5% of ablation. At another location near sea level, only 24% of ablation was calculated as being caused by radiation. This energy balance took the same form used in most energy balance studies since, and as presented by the US Corp of Engineers (1956) and Hock (2005) in their reviews of melt modelling:

$$H_N + H_H + H_L + H_G + H_R + H_M = 0 \quad (1)$$

Equation 1 shows the sum of net radiation (H_N), the sensible heat flux (H_H), the latent heat flux (H_L), the ground heat flux (H_G), the heat flux due to rain (H_R), and the energy consumed by melt (H_M) is zero. The net radiation includes incoming solar radiation (insolation) minus reflected solar radiation and absorbed minus emitted longwave radiation. The Turbulent heat

fluxes, H_H and H_L, were calculated using the gradient flux method, setting the flux proportional to the potential temperature gradient in the case of sensible heat and the specific humidity gradient in the case of latent heat. Svedrup (1935) was the first to apply the now commonly used gradient flux method to snow or ice (Hock, 2005). By convention, fluxes directed toward the snow or ice surface are positive. If snow is subfreezing, heat is required to bring its temperature up to the melting point before melt can begin. Melt can then be computed from the energy available for melt:

$$M = \frac{H_M}{\rho_w L_f} \tag{2}$$

Here M is the melt depth, ρ_w is the density of water, and L_f is the latent heat of fusion.

A detailed overview of energy-balance modelling for a snow surface is given by the Corp of Engineers (1956). The relative importance of the different energy-balance components varies with location: solar radiation may be more important in open terrain, but of less importance in forested areas and decreases in importance at higher latitudes. Because of the varying importance of different energy-balance components, there is no universally applicable index for snowmelt. The net heat flux is normally positive during the day and negative at night during the melt season. This often results in a snow crust as free liquid water in the top layers of the snowpack refreeze at night.

Clouds cause substantial variation in insolation values, but their effects are difficult to calculate. Slope also affects the intensity of insolation, with south (north) facing slopes receiving more insolation than north (south) facing slopes in the northern (southern) hemisphere. Tree canopies block insolation from reaching the underlying snow, with the magnitude of the effect

varying depending on the forest characteristics. Snow albedo varies considerably, with newly fallen snow reflecting around 80% of insolation, while older snow may reflect only 40%. Because snow is translucent, insolation is not only absorbed at the surface but penetrates to some depth in the snowpack. Snow is a near perfect blackbody in the case of longwave radiation, and so emits and absorbs radiation in accordance with the Stefan-Boltzmann law. Back radiation emitted by the earth's atmosphere, clouds, and trees also contributes to snowmelt (Corp of Engineers, 1956).

Calculation of snowmelt on a basin-wide scale is complicated even more by the spatial and temporal variability of the fluxes across the snow surface (Ferguson, 1999). Calculating the sensible heat flux requires air pressure, snow surface temperature, air temperature (which can have highly variable lapse rate), and wind speed (which varies with local topography). Net radiation depends on cloud cover, albedo, and shading effects from topography, which can be accounted for by using a digital elevation model (DEM). The data required to use such full energy balance method are often not available in most remote regions where it often needs to be applied (Day, 2009). Moreover, difficulties in extrapolating the numerous variables required for an energy balance model raises concern in the accuracy of distributed energy-balance models (Ferguson, 1999). While there are a few physically based snow models (e.g., CROCUS, SNTHERM, DAISY) (Hock, 2005), the data intensive nature of energy balance modelling and the difficulty in forecasting meteorological variables reduces the predictive ability of these models. These issues lead to the use of the degree-day model as an alternative method of calculating melt with less intensive data requirements.

2.3.2 Degree-Day Models

Degree-day models assume an empirical relationship between temperature and snow or ice melt. The close relationship between air temperature and melt rates was first described by Finsterwalder and Schunk (1887) and has since been refined and widely applied (Hock, 2003). Leach et al. (1933) compared plots of air temperature and runoff during a period of positive temperatures following a snow storm, noting high correlation between above freezing temperature and melt. Collins (1934) sought to utilize the degree day method in predicting water supply for Coeur d'Alene Lake, a storage reservoir in northern Idaho used for several hydroelectric projects. Below freezing temperatures were identified as having no effect on runoff, while above freezing temperatures correlated to melt, percolation, and evaporation. The study attempted to find a relation between positive degree days and runoff using data from three weather stations in the region. Multiple elevation bands were used with temperature interpolated to each band. Total accumulated degree days were weighted by the area of each band, then plotted against accumulated runoff as measured from USGS stream gauging stations. Accumulated runoff initially increased steeply and steadily with accumulated degree days before levelling off. A similar 'S' curve was produced by Wilson (1941), another study which plotted accumulated degree days against accumulated runoff. Rango and Martinec (1995) later noted the failure to account for snow cover area or runoff losses by the Collins (1934) study as the reason for the 'S' curve, with the first 500 degree days accounting for 85 percent of runoff.

Linsley (1943) outlines methods developed by the Weather Bureau office in Sacramento for forecasting discharge in the Sacramento and San Joaquin River basins in California. The

importance of determining the contribution of snowmelt to river discharge was noted, along with the usefulness of the degree-day model in determining melt given the lack of meteorological data for many regions beyond temperature and precipitation. Similar to Collins (1934), the elevation dependence of temperature was accounted for through the use of elevation bands. Degree day values were multiplied by the degree day factor (DDF) to give total melt over the basin. One potential method of determining the DDF is presented as dividing total runoff by accumulated degree days over a brief period during which there is little or no rain. The increase in the DDF throughout the melt season was noted, which was attributed to the ripening of the snowpack and variations in radiation or other melt factors. Rango and Martinec (1995) commented on the large seasonal increase in the degree day factor found by Linsley (1943), from 0.1 cm/°C/day to 0.7 cm/°C/day, as the result of flow recession not being taken into account (not all of the snowmelt appears immediately as runoff), in addition to the natural seasonal increase in the DDF.

Since these early studies related accumulated temperature directly to runoff, their approach ignored the depletion of the snowpack, runoff routing, and other hydrological processes. As in Linsley (1943), modern usage of the degree-day method also relates degree days to melt depth. However, the various models take different approaches in transforming calculated melt into runoff. The general form of the degree-day method is:

$$M = k(T_a - T_b), \qquad T_a > T_b \tag{3}$$

Where M is the melt depth, k is the degree day factor, T_a is the air temperature, and T_b is the reference temperature, usually 0°C. This method continues to be widely used because of the wide availability and relative ease of interpolating/forecasting air temperature; and strong

accuracy despite the simplicity of the relation (Hock, 2003; US Corp of Engineers, 1956). The high correlation between air temperature and other energy balance components make air temperature a useful index for calculating melt (Day, 2009). The degree-day method is especially effective in forested areas due to the reduced importance of insolation (U.S. Corp of Engineers, 1956). The method can produce comparable results to an energy balance model if applied correctly; the DDF must be adjusted through the melt season to account for its seasonal increase due to lower albedo and higher insolation (Rango and Martinec, 1995). The DDF is spatially and temporally variable, varying with local albedo, shading, slope and aspect, among other factors. Despite this variability, the degree-day method performs well in hydrological models, in part because of the smoothed response of runoff that provides some forgiveness to day to day errors in melt depth (Rango and Martinec, 1995).

The variability of the degree day factor and the fact that melt is influenced by many variables other than temperature has led to the formulation of enhanced degree-day models. Enhanced degree-day models often include net radiation or net shortwave radiation, given its importance to the energy budget of a snow surface. These models often assume the form:

$$M = kT + aR \tag{4}$$

Where R is the net radiation and a is a coefficient accounting for the contribution of radiation to melt. This approach has been applied in hydrological models including SRM, often yielding improved results over the base degree-day model (Hock, 2003).

2.3.3 Emergence of the Snowmelt Runoff Model (SRM)

Martinec (1960) found good correlation between the DDF and snow density and proposed a linear relationship between the two variables. Martinec (1963) expanded on this by attempting to model basin-wide snowmelt. Measured temperature was extrapolated to the mean elevation of the basin and used to calculate degree days. A lag time of 4 hours was determined using the observed lag between the rise in temperature and the rise in discharge. The recession in runoff was computed using:

$$Q = Q_0 e^{-kt} \tag{5}$$

Where Q is the discharge after time t, k is a coefficient representing the rate of flow recession, and Q_0 is the initial discharge. Daily runoff was then computed by applying the degree day method to calculate melt and adding the contributions from rain and recession flow from the previous day. This process of calculating snowmelt runoff was formally expressed by Martinec (1965):

$$Q_n = c[a_n T(1 - k) + Q_{n-1} k] \tag{6}$$

Where c is the runoff coefficient, T is the number of degree days, a is the degree day factor, k is the recession coefficient from equation (5), and n is an index expressed in days. This formulation was extended in Martinec (1970). The basin was divided into elevation bands with melt calculated separately for each band to account for differences in temperature and snow cover area with elevation. These changes brought the model near the form in which it was formally introduced as the Snowmelt Runoff Model by Martinec (1975), which introduced a recession coefficient which varied with discharge to account for increased basin responsiveness at higher flows. Martinec (1975) also added rainfall to the melt depth before applying the

recession coefficient to calculate runoff. The present form of the model includes separate runoff coefficients for snowmelt and rainfall:

$$Q_n = \sum_i (c_{Sin} a_{in} T_{in} SCA_{in} + c_{Rin} P_{in} RCA_{in}) (1 - k(x,y)_n) + Q_{n-1} k(x,y)_n \quad (7)$$

The discharge, Q, is calculated from the individual contributions of snowmelt, rainfall and recession from the previous day discharge. The temperature T is adjusted via a lapse rate to the hypsometric mean elevation of each elevation band. Temperature is multiplied by the degree day factor a to get depth of melt, and this is multiplied by the snow cover area SCA. The contribution of precipitation is calculated by multiplying the precipitation depth P by the rainfall contributing area RCA. The runoff coefficients c_S and c_R correspond to the ratio of snowmelt and rainfall to runoff, respectively, and account for losses such as evaporation and sublimation. It is recommended that if the study basin exceeds 500 metres in elevation range that it be divided into bands of about 500 m each to account for varying melt conditions (temperature and precipitation lapse rates). The snowmelt and rainfall contributions are calculated for each band individually and summed to obtain their total contribution. The index i is used to indicate the elevation zone. The sum of the snowmelt and rainfall contributions are then multiplied by the recession coefficient k, which expresses the decline in discharge during a period with no snowmelt or rainfall. This flow is then added to the recession flow from the previous day. The recession coefficient is a function of parameters x and y, accounting for the nonlinear response of the basin.

2.3.4 Remote Sensing of Snow Cover

Given the large areas occupied by snow cover, in situ measurements are insufficient for accurate mapping of snow extent. Remote sensing has allowed for the wide scale mapping of snow extent. The use of remote sensing in determining snow covered area began with air photos and has become increasingly practical with the abundance of satellite imagery. As air photos were generally used for topographic surveys, they were usually taken in late spring after snow cover had melted thus dedicated flights had to be flown to acquire snow cover data. The emergence of satellite imagery has provided an alternative for large scale observation and analysis of snow cover. The use of satellite imagery for snow cover analysis began in the 1960s. The first Landsat satellite was launched in 1972 (originally named the Earth Resources Technology Satellite), providing 90 m resolution at nadir and providing data for mid latitude regions every 18 days (Gray and Male, 1981). Following the launches of Landsat-1 and NOAA-2, deployed the same year, it was proposed that satellite data could be used in determining snow cover area and predicting snowmelt runoff (Rango, 1980). To this end, NASA carried out testing of satellite imagery utilization in operational runoff predictions under the Applications Systems Verification and Transfer (ASVT) program from 1975 to 1979. The use of satellite imagery was found to be valuable in reducing forecast error, with the use of snow cover imagery in SRM reducing flow estimate errors by 10-15% for three basins in California (Rango, 1980). The use of satellites in operational snowmelt forecasting at the time was limited by the long lag time between data acquisition and delivery to the end user, as well as infrequent coverage at acceptable resolutions.

Snow has distinctive characteristics in the visible, near infrared, and microwave portions of the electromagnetic spectrum that allow for its detection through remotely sensed imagery. Optical imagery can be used to obtain much higher spatial resolution than passive microwave imagery but is limited by hours of daylight and presence of cloud cover. A common approach to detecting snow is to use two spectral bands: one centred in the visible part of the spectrum, and one centred in the near infrared around 1.65 µm. These bands are used for snow identification because while clouds and snow have similar reflectance below 1 µm, their reflectance diverges and achieves a maximum difference in the near infrared (Meier, 1980). Snow cover is typically identified using the Normalized Difference Snow Index (NDSI):

$$NDSI = \frac{r_{vs} - r_{ir}}{r_{vs} + r_{ir}} \tag{8}$$

With r_{vs} and r_{ir} being the visible and shortwave infrared reflectance, respectively. For Landsat, bands 2 (visible) and 5 (infrared) are used while for Moderate Resolution Imaging Spectrometer (MODIS), band 4 (visible) and 6 (infrared) are used. An NDSI greater than 0.4 is used to indicate snow cover. Additional criteria that the reflectance of the visible band be greater than 0.11 and the reflectance of the infrared band be greater than 0.10 prevent misidentification of water as snow, as water also tends to have high NDSI values. (Rees, 2005)

Snow cover maps have been available since 1966, derived from data from NOAA's GOES and POES satellites. These weekly charts of the northern hemisphere had a spatial resolution of 190 km (Hall et al., 1996). Since the launch of the NOAA Advanced Very High Resolution Radiometer (NOAA-AVHRR), we have had the ability to observe daily snow cover on a continuous basis at 1.1 km resolution. This resolution is still too coarse for hydrological modelling in smaller basins

but can be used over larger areas and for climate studies (Rango, 1996). Following the launch of MODIS in 1999, NASA has been producing global daily snow cover maps at 500-meter resolution using MODIS imagery. An 8-day composite snow cover product is produced from these daily products to minimize cloud cover and obtain the greatest snow cover extent over the 8-day period (Hall et al., 2002).

Most hydrological models (HBV, NWS, UBC, SHE) simulate the growth and decay of the snowpack (Hock, 2005), whereas SRM takes advantage of satellite imagery in determining snow cover area. Temperature is used in those models to determine whether precipitation falls as rain or snow. Meteorological stations are sparse in high elevation regions (EDW Working Group, 2015), and it is necessary to extrapolate temperature and precipitation across the study basin to simulate snowpack. Temperature and precipitation are also spatially variable and should be adjusted with elevation using temperature and precipitation lapse rates. Despite temporal and spatial variations in temperature lapse rates, most models use a fixed lapse rate, which can introduce large errors in temperature for basins with a large elevation range (Blöschl, 1991). Precipitation can be highly localized and most gauges systematically under catch snow, particularly in windy conditions, which can be problematic for models which model the growth of the snowpack (Ferguson, 1999). A model can accurately calculate melt rates but still give poor runoff estimates if there is error in the snow cover area. Thus models that model snowpack growth can give erroneous results not through a fault in the model itself, but through uncertainty in meteorological variables leading to inaccurate snow cover area. SRM reduces the error involved in modelling snowpack growth by using satellite imagery to determine actual

snow cover. However, when used in forecast mode, SRM must rely on snow cover data from previous years to extrapolate SCA into the future.

2.4 Review of the Application of SRM

SRM has been applied to over 100 basins, ranging in size from 0.76 to 917,444 km^2 (Martinec et al., 2008). Initially applied to small European basins, the model has since been applied to snow covered regions worldwide. A list of basins where SRM is used is provided by Martinec et al. (2008). SRM has been used in many of the mountainous regions of Europe, Canada, and the USA. In the southern hemisphere it has been applied in several basins within the Andes, as well as in New Zealand and Australia. It has also been used in various locations throughout the Himalayas, China, and Japan. SRM has recently begun being applied in northwestern China, where its limited meteorological data requirements are advantageous given the sparsity of hydro-meteorological data in the region (Abudu et al., 2012).

Various enhancements to SRM have been tested since its introduction. The addition of a radiation component to the melt calculation is a common enhancement for improving model performance (e.g. Brubaker et al., 1996; Li and Williams, 2008; Vafakhah et al., 2014). These studies often divide their study basins into aspect zones as well as elevation zones to account for spatial variations in received insolation. Alternatively, Abudu et al. (2016) applied set temperature adjustments to different aspect and slope classes to account for topographic effects on melt without explicitly modelling radiation. Harshburger et al. (2010, 2012) used an enhanced version of SRM which incorporates an antecedent temperature index method to track the ripeness of the snowpack and minimum and maximum critical temperatures to

partition precipitation into rain, snow, and a rain snow mix. Both enhancements improved model performance.

2.4.1 Short-Term Forecasting and Climate Change Scenarios

SRM has been applied to both short term forecasting and climate change studies. Short-term runoff forecasts utilizing SRM have been shown to be useful up to a six-day lead time (Nagler et al., 2008) with forecast skill declining with lead time (Harshburger et al., 2010). This reduced forecast skill can be at least partially attributed to error in weather forecasts. Temperature and precipitation from short term forecasts or climate change projections is used as model input, leaving only snow cover area to be determined. SRM can extrapolate SCA using Modified Depletion Curve (MDC). An MDC is produced by creating a relationship between SCA and cumulative snowmelt depth using historical data. A family of MDCs can be produced from multiple years of historical data. To extrapolate melt, an MDC with similar snow conditions to the study period is selected, and SCA is extrapolated using the MDC to determine what SCA is associated with the forecasted cumulative melt depth.

SRM includes a built-in climate-scenario module to simulate year-round stream flow under a changed climate (Martinec et al., 2008). Rango and Martinec (1997) quantified the seasonal shift in runoff due to warmer temperature for the Rio Grande basin in Colorado. A wet year, dry year, and average year were utilized in creating MDCs, which were used to simulate the effects of a 4°C temperature increase. Precipitation was assumed to remain the same thus annual runoff remained little changed, but there was a shift toward increased winter runoff at the expense of summer runoff. Seidel et al. (2000) apply SRM to the Ganges and Brahmaputra

basins, and simulate runoff under a temperature increase of 1.5°C and a 10% increase in precipitation. These are the largest basins in which SRM has been applied, at 917,444 km^2 and 547,346 km^2, respectively. The simulated climatic changes were found to increase peak runoff during flooding by 20% for the Ganges and 30% for the Brahmaputra, while April-December runoff volume increased by 25% for both basins. Seidel et al. (2008) simulated the effects of climate change on the 3250 km^2 Rhine-Felsberg basin in the Swiss Alps, finding more summer flooding events as summer snowfalls were replaced by rain.

Despite the MDC methodology for estimating future snow cover developed for SRM, several studies opt to instead use a range of prescribed changes to SCA. Ma et al. (2013) utilized downscaled GCM output to develop multiple climate change scenarios for the Kaidu watershed in northwestern China. These scenarios included keeping SCA the same as the historical climate and evaluating the effects of both increases and decreases in SCA on runoff. Tahir et al. (2011) examined the effects of a changed climate on flow rates in the Hunza River basin in Pakistan. Three climate change scenarios were examined: a temperature increase of 4°C; a 20% increase in cryosphere area until 2075 and 10% increase until 2050, assumed based on increased precipitation; and a third scenario combining increased temperature with increased cryosphere area. Nolin et al. (2010) examined the effects of climate change on a glacierized basin, assessing multiple prescribed reductions in glacier area.

Few SRM studies have explicitly accounted for glaciers, despite the model's frequent use in mountainous glacierized basins. Schaper and Seidel (2000) applied separate glacier and snow DDFs in SRM to a climate change study of three basins in Switzerland. Glacier area was reduced for the warming climate based on an equilibrium line shift calculated from the increase in

summer temperature. Rango et al. (2008) examined the effects of a warmed climate on stream flow in the glaciated Illecillewaet basin in British Columbia. The higher DDF for glacial ice was accounted for using the minimum observed SCA as an estimate of glacier area. For a non-glaciated basin, an increase in temperature would shift peak runoff earlier in the season, while total runoff would remain the same (assuming seasonal snow cover and precipitation remain unchanged). This is not true of a glaciated basin, where there will be increased runoff due to glacial melt. This study did not account for glacial retreat due to increased melt, resulting in overestimated projected runoff. Nolin et al. (2010) apply SRM to a glacierized catchment in the Pacific Northwest. Glacier area was used in place of snow cover area in the traditional SRM setup, with snow cover accounted for through precipitation and temperature. Separate DDFs for snow and ice were utilized.

2.5 Advantages and Disadvantages of Using SRM

The Snowmelt Runoff Model is built around the remote sensing of snow cover and the use of the degree day model. As previously discussed, degree day models have the advantage of requiring only temperature to calculate snow melt while producing results comparable to those of an energy balance model for many hydrological applications. Degree day models have been commonly used throughout the history of snow melt modelling due to the wide availability of temperature data and the relative sparseness of measurements for other meteorological variables which would be required to do a full energy-balance model. Temperature is also relatively easy to interpolate, and degree-day models avoid the error involved in requiring other meteorological variables which may be more difficult to interpolate. The use of

temperature as the sole index of melt can be problematic, however, as it is one of many factors influencing melt and so the degree-day factor must be varied to account for the changing relative contributions of the various energy-balance components. The degree-day factor gradually increases through the melt season for multiple reasons including increasing insolation, decreasing albedo, and the ripening of the snowpack. The degree-day factor also varies spatially due to the aspect of the snow surface, shading from surrounding topography, and elevational effects on energy-balance components (e.g., temperature decreasing with elevation). For a degree-day model to be applied in hydrological modelling, an average basin-wide DDF must be determined. The ease of forecasting temperature is also an advantage for forecasting streamflow, as other variables are more difficult to forecast.

The sparseness of meteorological data in the high-elevation regions in which SRM is often applied and the difficulty in interpolating this data make the simulation of snow-cover area problematic. Accurate snow-cover area is important for runoff modelling as errors in calculated snowmelt will be proportional to the error in snow-covered area. Models that simulate the snowpack may encounter issues with small-scale processes such as blowing snow, but even if the model were perfect, it may still produce erroneous results due to inaccurate meteorological data. The use of satellite imagery in SRM to determine snow-cover area avoids the uncertainty involved in modelling the snowpack. This approach comes with its own flaws. Infrequent satellite imagery or the presence of cloud cover may prevent the mapping of snow cover for periods of time, and resolution must be sufficiently high to accurately map snow cover for a basin, with smaller basins requiring higher resolution imagery (Day, 2009).

In a review of several runoff models, Day (2009) noted that while SRM requires less calibration than other models, it should not be applied to basins without historical discharge records to calibrate the model. These parameters include the runoff coefficient, which can be calculated as the long term ratio between precipitation and runoff; lag time, which can be determined by examining the lag between a rise in temperature and a rise in discharge; and the recession coefficient, which can be determined by plotting discharge on for each day against discharge on the following day. While its developers do not consider SRM to be a calibration model and state parameter values should be selected based on hydrological judgements, in practice, parameter values often require adjusting to provide accurate results (Ferguson, 1999). The runoff coefficients account for losses due to evapotranspiration and are varied temporally to account for changes in losses over time. In practice, these coefficients are often used to correct for systematic errors in modelled runoff (Ferguson, 1999).

SRM takes a minimalist approach to runoff routing and does not explicitly model groundwater. Most runoff models represent flow routing through a series of reservoirs, where outflow from a reservoir is modeled as some function of the volume of water in that reservoir (Ferguson, 1999). Separate reservoirs may be used to represent surface flow, interflow and groundwater. SRM features the simplest representation of runoff routing, using a single non-linear reservoir. The use of a non-linear reservoir allows SRM to capture the increased responsiveness of a basin hydrograph at high flows, but the single reservoir approach lacks the ability to fit the same range of conditions as a model with a more detailed representation of runoff routing.

2.6 Summary

A substantial portion of the world's population lives in regions in which streamflow is dominated by snowmelt runoff. As the climate changes and snowpacks shrink, there will be reduced summer flows and increased runoff in the winter and spring. Modelling runoff is important for managing water resources, as shifts in runoff patterns impact irrigation, hydroelectric projects, stream ecology, and industrial and municipal use of water.

Snow accumulates at high latitudes and high elevations through the fall and winter, before being released as meltwater in the spring. Several energy fluxes contribute to the energy balance of the snowpack, with the largest contributors being the radiative and turbulent heat fluxes. Because of the sparseness of observations and difficulty in interpolating or forecasting many of the required variables, temperature-index models are often used instead. Temperature functions well as the sole index of melt because it is closely correlated with other melt factors such as net radiation.

The remote sensing of snow covered area has allowed for more accurate assessment of snowmelt runoff. Though the Snowmelt Runoff Model was originally developed before widespread satellite imagery at a resolution useful to runoff modelling, the increased frequency and resolution of satellite imagery has allowed SRM to become a frequently used hydrological model for snow-covered regions. Originally developed for simulating flow for small European basins, SRM has since been applied to basins around the world. The model has been used in conjunction with meteorological forecasts for producing short-term runoff forecasts as well as with GCM output for climate-change impact studies.

References

Abudu, S., Cui, C., Saydi, M., & King, J. P. (2012). Application of snowmelt runoff model (SRM) in mountainous watersheds: A review. Water Science and Engineering, 5(2), 123–136.

Abudu, S., Sheng, Z. ping, Cui, C. liang, Saydi, M., Sabzi, H. Z., & King, J. P. (2016). Integration of aspect and slope in snowmelt runoff modeling in a mountain watershed. Water Science and Engineering, 9(4), 265–273.

Barnett, T. P., Adam, J. C., & Lettenmaier, D. P. (2005). Potential impacts of a warming climate on water availability in snow-dominated regions. Nature, 438(7066), 303–309.

Baumgartner, M. F., Spreafico, M., & Weiss, H. W. (2000). Operational snowmelt runoff forecasting in the Central Asian mountains. Remote Sensing and Hydrology, 267(267), 66–71.

Blöschl, G. (1991). The Influence of Uncertainty in Air Temperature and Albedo on Snowmelt. Nordic Hydrology, 22(2), 95–108.

Brubaker, K., Rango, a, & Kustas, W. (1996). Incorporating radiation inputs into the snowmelt runoff model. Hydrological Processes, 10(April), 1329–1343.

Bruce, J. P., & Clark, R. H. (1966). Introduction to hydrometeorology. Oxford: Pergamon Press.

Collins, E. H. (1934). Relationship of degree-days above freezing to runoff. In Eos, Transactions American Geophysical Union (pp. 624–629).

Day, C. (2009). Modelling impacts of climate change on snowmelt runoff generation and streamflow across western US mountain basins: a review of techniques and applications for water resource management. Progress in Physical Geography, 33(5), 614–633.

EDW Working Group (2015). Elevation-dependent warming in mountain regions of the world. Nature Climate Change, 5(5), 424–430.

Ferguson, R. I. (1999). Snowmelt runoff models. Progress in Physical Geography, 23, 205–227.

Forster, E. E. (1948). Rainfall and run-off.

Gómez-Landesa, E., & Rango, a. (2002). Operational snowmelt runoff forecasting in the Spanish Pyrenees using the snowmelt runoff model. Hydrological Processes, 16(8), 1583–1591.

Gray, D. M., & Male, D. H. (1981). Handbook of snow: Principles, processes, management & use. Toronto: Pergamon Press.

Hall, D. K., Riggs, G. a., Salomonson, V. V., DiGirolamo, N. E., & Bayr, K. J. (2002). MODIS snow-cover products. Remote Sensing of Environment, 83(1-2), 181–194.

Harshburger, B. J., Humes, K. S., Walden, V. P., Moore, B. C., Blandford, T. R., & Rango, A. (2010). Evaluation of short-to-medium range streamflow forecasts obtained using an enhanced version of SRM1. Journal of the American Water Resources Association, 46(3), 603–617.

Harshburger, B. J., Walden, V. P., Humes, K. S., Moore, B. C., Blandford, T. R., & Rango, A. (2012). Generation of Ensemble Streamflow Forecasts Using an Enhanced Version of the Snowmelt Runoff Model. Journal of the American Water Resources Association, 48(4), 643–655.

Hock, R. (2005). Glacier melt: a review of processes and their modelling. Progress in Physical Geography, 29(3), 362–391.

Hock, R. (2003). Temperature index melt modelling in mountain areas. Journal of Hydrology, 282(1-4), 104–115.

Leach, H. R., Cook, H. L., & Horton, R. E. (1933). Storm-Flow Prediction. Trans. A.G.U., 435

Li, X., & Williams, M. W. (2008). Snowmelt runoff modelling in an arid mountain watershed, Tarim Basin, China. Hydrological Processes, 22, 3931–3940.

Linsley, R. K. (1943). A Simple Procedure for the Day-to-Day Forecasting of Runoff From Snow-Melt. In Eos, Transactions American Geophysical Union, 24, 62–67.

Ma, Y., Huang, Y., Chen, X., Li, Y., & Bao, A. (2013). Modelling snowmelt runoff under climate change scenarios in an ungauged mountainous watershed, Northwest China. Mathematical Problems in Engineering.

Martinec, J. (1960) The degree-day factor for snowmelt-runoff forecasting, IUGG General Assembly of Helsinki, IAHS Publ. No. 51, Surface Waters, pp. 468-477.

Martinec, J. (1963). A representative watershed for the research of snowmelt-runoff relations. International Association of Scientific Hydrology.

Martinec, J. (1963) Forecasting Streamflow from Snow Storage in an Experimental Watershed, IASH General Assembly of Berkeley 1963, Commission of Surface Waters.

Martinec, J. (1970). Study of Snowmelt Runoff Process in Two Representative Watersheds with Different Elevation Range. In International Symposium on the results of research on representative and experimental basins, Wellington, IAHS Publ. No. 96 (pp. 29–39).

Martinec, J. (1975). Snowmelt - runoff model for stream flow forecasts. Nordic Hydrology, 6(3), 145–154.

Martinec, J., et al. (2007), Snowmelt Runoff Model (SRM): User's Manual, 175 pp., N. M. State Univ., Las Cruces.

Mountain Research Initiative EDW Working Group (2015). Elevation-dependent warming in mountain regions of the world. Nature Clim. Change, 5(5), 424–430.

Nagler, T., Rott, H., Malcher, P., & Müller, F. (2008). Assimilation of meteorological and remote sensing data for snowmelt runoff forecasting. Remote Sensing of Environment, 112(4), 1408–1420.

Nolin, A. W., Phillippe, J., Jefferson, A., & Lewis, S. L. (2010). Present-day and future contributions of glacier runoff to summertime flows in a Pacific Northwest watershed: Implications for water resources. Water Resources Research, 46(12), 1–14.

Rango, A. (1980). Operational Applications of Satellite Snow Cover Observations. Journal of the American Water Resources Association, 16(6), 1066–1073.

Rango, a. (1996). Spaceborne remote sensing for snow hydrology applications. Hydrological Sciences Journal, 41(4), 477–494.

Rango, A., & Martinec, J. (1995). Revisiting the degree-day method for snowmelt computations. Water Resources Bulletin, 31(4), 657–669.

Rango, A., & Martinec, J. (1997). Water storage in mountain basins from satellite snow cover monitoring. IAHS Publications, (242).

Rango, A., Martinec, J., & Roberts, R. (2008). Relative importance of glacier contributions to water supply in a changing climate. World Resource Review, 20(3), 487–503.

Rango, A., & van Katwijk, V. (1990). Development and testing of a snowmelt-runoff forecasting technique. Water Resources Research, 26(1), 135–144.

Rees, W. G. (2005). Remote sensing of snow and ice. CRC Press.

Schaper, J., & Seidel, K. (2000). Modelling Daily Runoff From Snow and Glacier Melt Using Remote Sensing Data. Proceeding of EARSeL-SIG-Workshop Land Ice and Snow, 1, 308–317.

Seidel, K., Ehrler, C., & Martinec, J. (1998). Effects of climate change on water resources and runoff in an Alpine basin. Hydrological Processes, 12(October), 1659–1669.

Seidel, K., Martinec, J., & Baumgartner, M. F. (2000). Modelling Runoff and Impact of Climate Change in Large Himalayan Basins. Islam Zeitschrift Für Geschichte Und Kultur Des Islamischen Orients, 1–9.

Şensoy, A., & Uysal, G. (2012). The Value of Snow Depletion Forecasting Methods Towards Operational Snowmelt Runoff Estimation Using MODIS and Numerical Weather Prediction Data. Water Resources Management, 26(12), 3415–3440.

Sverdrup, H. U., & Ahlmann, H. W. (1935). Norwegian-Swedish Spitsbergen Expedition in 1934. Geografiska Annaler, 18(1935), 34–73.

Tahir, A. A., Chevallier, P., Arnaud, Y., Neppel, L., & Ahmad, B. (2011). Modeling snowmelt-runoff under climate scenarios in the Hunza River basin, Karakoram Range, Northern Pakistan. Journal of Hydrology, 409(1-2), 104–117.

United States. Army. Corps of Engineers. (1956). Snow hydrology: summary report of the snow investigations. Portland, Or.: North Pacific Division, Corps of Engineers, U.S. Army.

Vafakhah, M., Nouri, A., & Alavipanah, S. K. (2014). Snowmelt-runoff estimation using radiation SRM model in Taleghan watershed. Environmental Earth Sciences, 73, 993–1003.

3 Chapter 3: Snowmelt Runoff Modelling for the Upper Athabasca River

Abstract

The Snowmelt Runoff Model (SRM) is a widely used hydrological model for simulating runoff in snowmelt dominated mountainous basins due to its relative simplicity and the accuracy provided by utilizing remotely sensed snow-cover imagery to determine snow-cover extent, avoiding the error associated with modelling the snowpack. Remotely sensed snow-cover is combined with the temperature-based degree day method for simulating snowmelt, an advantageous approach in mountainous regions where meteorological observations are sparse and difficult to interpolate. The degree-day method calculates melt by relating the mean daily temperature to melt depth through the degree-day factor (DDF), a coefficient obtained through measurement or calibration. Despite being widely applied in glaciated basins, SRM studies have rarely explicitly accounted for the difference in DDF between glacier ice and snow, instead applying a zonal (elevation dependent) DDF. SRM was calibrated for the Upper Athabasca River Basin with separate snow and ice DDFs, satisfactorily simulating flows over the calibration (2000-2002, average NSE of .93) and validation (2003-2010, average NSE of .88) periods. The glacier DDF model produced comparable results to that of the zonal model. Zonal model calibration produced DDF values consistent with glaciers being the largest drivers of DDF elevation dependence. Accounting for the higher glacier DDF, either explicitly or through elevation dependence, was found to be essential in capturing interannual variability in melt conditions.

3.1 Introduction

Streamflow forecasts are valuable source of information for water resource management. Runoff predictions can be used to assess water availability for irrigation, hydroelectricity generation, and municipal or industrial use (Ferguson, 1999). For most regions north of 45°N and mountainous regions at lower latitudes, this runoff is primarily derived from snowmelt (Barnett, 2005). In snowmelt dominated regions, changing temperatures are of greater interest to forecasting flow than precipitation, as it is temperature that governs the timing and magnitude of meltwater (Arnell, 1999). The reduction of the winter snowpack and resulting reduction in summer runoff is of importance to regions such as the Canadian Prairies, where water usage peaks in the summer due to demand for irrigation and municipal water withdrawals (Schindler and Donahue, 2006). Although climate change is expected to intensify the hydrological cycle, increasing global average precipitation, large regions will experience reductions in precipitation (Arnell, 1999). Changes in seasonal runoff patterns over the last century have been observed in numerous rivers originating in the Rocky Mountains, with an analysis of 14 rivers located throughout the Canadian and Northern USA Rocky Mountains finding an increasing trend in winter flows and a decreasing trend in summer flows (Rood et al., 2008). Quantifying future runoff will assist water consumers in preparing for changing runoff seasonality.

With runoff in the Canadian Rocky Mountains dominated by snowmelt, it is essential that snowpack processes be modelled accurately. Both the accumulation of the winter snowpack and its subsequent release as melt water in the spring must be properly captured, both of which present challenges in mountain environments where meteorological conditions are

spatially variable and observations can be sparse. Precipitation can be highly localized, leading to difficulties in accurately quantifying basin-wide runoff without a dense network of precipitation gauges (Faurès et al., 1995). This uncertainty in precipitation will affect both modelled rainfall runoff and modelled snow accumulation. Additional uncertainty in modelling snow accumulation stems from the use of a static temperature threshold to differentiate snow from rain. Identical near-surface air temperatures could result in either rain or snow depending on the local lapse rate, which will vary depending on atmospheric conditions (Feiccabrino et al., 2015). Wind and slides act to redistribute snow once it has fallen, resulting in heterogeneous snow cover. Many hydrological models attempt to simulate the accumulation and distribution of snowfall (e.g. HBV), while others avoid the uncertainty in modelling the snowpack by using remotely sensed snow cover imagery (Ferguson, 1999).

The contribution of melt to runoff can be modelled using the energy-balance or degree-day methods. Energy-balance modelling is a physically based approach in which the various heat fluxes into the snow or ice surface are quantified. This approach is data intensive, requiring vertical temperature and specific humidity gradients, wind speed, shortwave and longwave incoming and outgoing radiation, and precipitation (Hock, 2005). Hence, degree-day models have developed in response to the high data requirements and computational complexity of energy balance models. While net radiation tends to be the largest heat flux, the close relationship between temperature and other energy-balance components allows temperature to be used as a relatively accurate index for melt estimation. Taking advantage of the high correlation between temperature and melt, degree-day models assume a linear relationship between the two variables (Hock, 2003). The degree-day method is utilized in many

hydrological models as it can obtain similar accuracy in results to energy-balance models despite its simplicity and light data requirements (Rango and Martinec, 1995).

This degree day – melt relationship, however, varies both temporally and spatially reflecting changing relative contributions of the different energy fluxes. Slope and aspect affect the amount of insolation a given point on the snowpack receives. Tree cover reduces the influence of the turbulent heat fluxes and enhances long wave radiation relative to open terrain (Woo and Giesbrecht, 2000). The degree day factor (DDF), a coefficient relating temperature to melt depth, tends to be larger at higher elevations due to the increased relative contribution of radiation (Hock, 2003). DDF also tend to be higher for glaciers due to the lower albedo of ice relative to snow. These spatial variations in melt conditions may impact the ability of a single basin wide melt factor to accurately model snowmelt runoff. The DDF varies temporally both on a daily timescale and a seasonal timescale, with day-to-day fluctuations due to changing meteorological conditions. Despite this day-to-day variability, when averaged over several days the DDF is much more consistent, and the smoothed response of runoff to snowmelt events allows some forgiveness to daily errors in melt quantity (Hock, 2003; Martinec et al., 2008). Seasonally, the DDF increases throughout the spring from the increased contribution of radiation and decreasing albedo of the snowpack. Accounting for these seasonal changes is vital to accurately modelling snowmelt runoff (Rango and Martinec, 1995).

The Snowmelt Runoff Model (SRM) is a conceptual hydrological model for simulating runoff in snowmelt dominated basins. SRM has been applied in over 100 basins worldwide, ranging in size from under 1 km^2 to over 900,000 km^2 (Martinec et al., 2008). Modelling of snowmelt runoff is simplified by utilizing remotely sensed snow cover imagery rather than simulating

snow accumulation and redistribution; and using a degree-day model rather than a more data intensive energy-balance model. While many other models utilize the degree-day approach, the advantage of SRM is in its incorporation of remotely sensed imagery, reducing error normally associated with modelling the snowpack.This approach results in only three required input variables which are relatively widely available: temperature, precipitation, and snow cover area. SRM is shown to produce satisfactory results despite its simplicity, making it an ideal model for determining streamflow in mountainous regions where data may be lacking (Day, 2009; EDW Working Group, 2015). However, most SRM studies in glacierized basins have not explicitly accounted for separate melt factors for snow and ice, though many use separate DDFs for each elevation band (e.g., Tahir et al., 2011; Ma et al., 2013). Increasing the DDF with elevation would account for more extensive glacier cover and the higher DDF for snow due to the increased relative contribution of solar radiation to melt (Hock, 2003). This study utilizes SRM in simulating runoff for the Upper Athabasca River Basin at Hinton. The importance of seasonal, elevational, and glacial variations in DDF is examined through comparison of several approaches to handling the DDF. The DDF and other parameters were determined solely through calibration within a range of physically plausible values, testing (validating) the ability of each model approach to realistically simulate the basin hydrograph in the absence of field measurements to inform parameter value selection.

Parameters for SRM are intended to be physically based, with parameter values chosen based on basin characteristics and historical data (Martinec et al., 2008). In practice, the physical basis of these parameters is weak, and some calibration is often necessary to obtain acceptable results. As with all conceptual hydrological models, the simplification and spatial aggregation of

hydrological processes results in parameters which cannot be directly measured or obtained through theory (Ferguson, 1999; Liu and Gupta, 2007). Instead, models are calibrated by tuning parameters through a range of physically plausible values to maximize model fit. This lack of a definitive, measurable parameter set leads to the concept of equifinality, where many different model structures and parameter sets can produce acceptable representations of the behaviour of a system (Beven and Freer, 2001).

Estimating parameter uncertainty is typically handled using data assimilation (Liu and Gupta, 2007), a general term which refers to mathematical techniques which combine observations with a model. Bayes theorem has been employed as the foundation of many of these data assimilation methods (Liu and Gupta, 2007), simultaneously allowing for the calibration of hydrological models while accounting for prior knowledge of the system, and producing uncertainty estimates for parameter values, state variables, and model output. The Markov Chain Monte Carlo (MCMC) technique is one such data assimilation algorithm which has previously been applied to SRM (Panday et al., 2014). The MCMC Metropolis algorithm is utilized in this study for model calibration and assessing parameter uncertainty.

3.2 Study Area and Data

3.2.1 Study Area Description

The study region is the Upper Athabasca River Basin in the Albertan Rockies of Canada, roughly coterminous with Jasper National Park. Flow is simulated for the hydrometric station in Hinton, about 25 km downstream from the park boundary. The 9760 km^2 watershed is characterized by mountainous terrain, with elevations ranging from approximately 960 m to 3740 metres above

sea level. The basin spans in latitude from 52°07’ N to 53°29’ N and in longitude from 117°06’ W to 119°04’ W. This region experiences a subarctic climate, with subfreezing mean daily temperatures five months of the year at lower elevations and longer higher up. Coniferous forest covers much of the basin below 2200 m elevation, above which summer temperatures are insufficient to allow for tree growth. Glacier cover is about 3% of the watershed and is concentrated around the southern portion of the basin, including a portion of the Columbia Icefield.

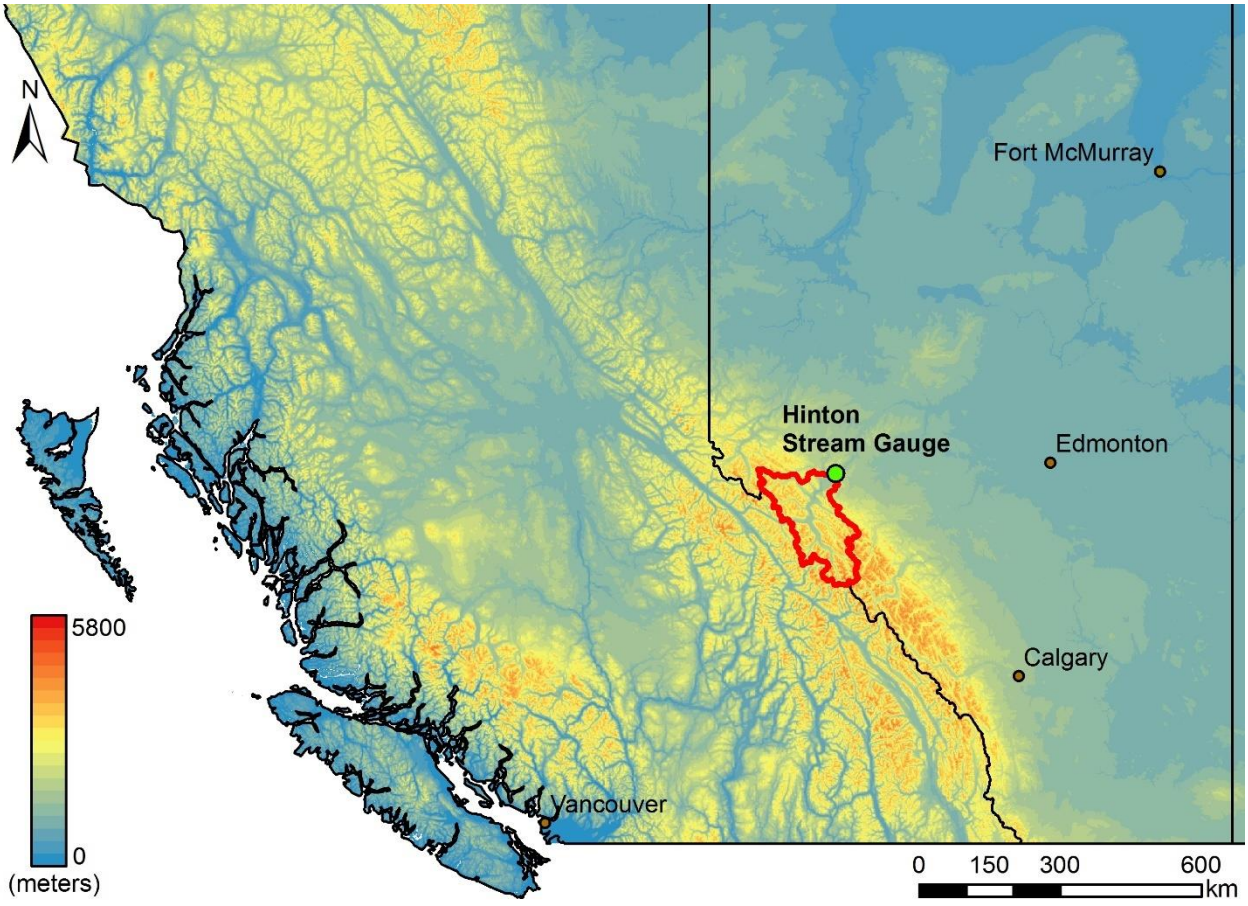

Figure 1: Location of Study Area (outlined in red)

3.2.2 Data sets

Historical temperature and precipitation data were derived from the ANUSPLIN dataset for Canada (Hutchinson et al., 2009). This product utilizes daily minimum and maximum temperature and precipitation data from Environment Canada weather stations across Canada. A trivariate thin plate smoothing spline was applied to interpolate these variables down to a 300 arc second grid (~10 km) based on high resolution DEM acquired from NRCan. Details on the methods and validation of the ANUSPLIN dataset can be found in Hutchinson et al. (2009). The Canadian Digital Elevation Model (CDEM), providing 0.75 second (~20 m) resolution elevation data for the Athabasca River Basin, was acquired from the geogratis.gc.ca website.

Snow cover data were derived from the MOD10 Snow product, produced by the National Snow and Ice Data Center (NSIDC). The MOD10 snow product uses data collected by the Moderate Resolution Imaging Spectroradiometer (MODIS) aboard the Earth Observing System (EOS) Terra spacecraft. MODIS snow products provide daily 500-m resolution images with global coverage. While alternative remote sensing products such as Landsat ETM+ may provide higher spatial resolution, while poor temporal resolution causes these products to miss short-term changes in snow cover extent, and available images may be obscured by cloud. MODIS is frequently utilized in SRM applications (e.g. Abudu et al., 2016; Vafakhah et al., 2014; Georgievski, 2009; Li and Williams, 2008) as its daily repeat period means it is more likely to capture cloud free imagery. The automated algorithm for producing the snow cover product utilizes the normalized difference snow index (NDSI) to determine the presence of snow:

$$NDSI = \frac{band\ 4 - band\ 6}{band\ 4 + band\ 6} \quad (1)$$

This calculation requires the satellite reflectance in MODIS bands 4 (.545-.565 µm) and 6 (1.628-1.652 µm). A pixel is mapped as snow if it has a NDSI greater than 0.4, a band 2 (.841-.876 µm) reflectance > 11%, and a band 4 reflectance > 10%. The band 4 minimum reflectance prevents dark pixels with erroneously high NDSI values due to the small denominator from being classified as snow. The Normalized Difference Vegetation Index (NDVI) is also utilized: If the NDVI is low (~0.1), indicating a lack of vegetation, a pixel may be mapped as snow even with a NDSI < 0.4. Finally, a thermal test is applied to remove erroneous snow values, requiring snow covered pixels to have a temperature below 283 K (Hall et al., 2002). In addition to the snow presence, a sub pixel snow fraction product was introduced in September 2006. Sub pixel snow cover fraction is calculated using a linear relationship between snow cover fraction and NDSI:

$$fraction = -0.01 + 1.45 \times NDSI \quad (2)$$

The snow cover data used were processed imagery derived from the MOD10A1.5 products, processed by Fitzharris and Sirguey (2014). The MOD10A1.5 product was downloaded for the dates February 24, 2000 to December 31, 2011. The 500 m resolution data were re-projected into the NAD83(CSRS) 10TM (Forest) cartographic system at 250 m resolution using nearest neighbor sampling. Cloud covered pixels were filled by temporally interpolating snow cover fraction for each pixel using a cubic smoothing spline. As MODIS was launched in 1999, only years from 2000 onward could be modelled with this approach.

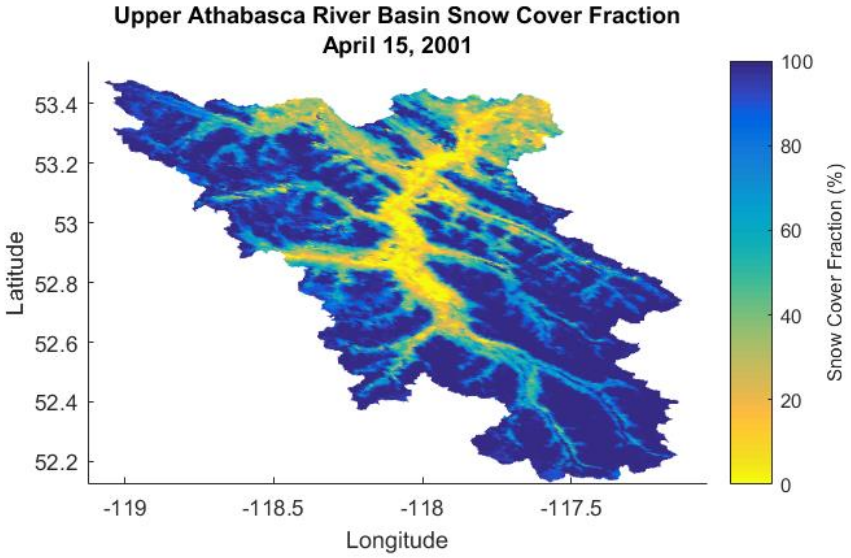

Figure 2: Example snow cover map for the study area

Glacier covered area was assumed to be equal to the minimum observed SCA from the MODIS SCA data. Glacier outlines from the Global Land Ice Measurements from Space (GLIMS) inventory were obtained for the study region for comparison with the MODIS SCA minimum estimate of glacier area (Raup et al., 2007; Bolch, 2008). Discharge data were obtained from the Environment Canada hydrometric database (HyDat). Data from the hydrometric station near Hinton, a town on the Athabasca River just downstream from Jasper National Park, were used. ECCC hydrometric stations continuously log river stage and use a stage-flow relationship to calculate discharge.

3.3 Methods

The Snowmelt Runoff Model was implemented in MATLAB and applied to simulating runoff for the Upper Athabasca river Basin at Hinton, building upon the work of Fitzharris and Sirguey

(2014) who found SRM to perform well in reproducing observed flows in this basin. SRM requires only three variables to simulate stream flow: temperature, precipitation, and snow cover area. Requiring only these three widely available variables make SRM ideal for studies where measurements of other variables are lacking. SRM divides the watershed into elevation bands, over which snowmelt and rainfall contributions to runoff are calculated. Averaging meteorological variables over elevation bands accounts for the elevation dependence of those variables, while reducing computational time over a fully distributed model where runoff contributions may be calculated over hundreds of thousands of pixels. The basin was broken up into five elevation bands (Figure 4) with each variable averaged over the elevation zone to produce zonal temperature, precipitation, and snow cover values for each day. Calculated temperature lapse rates were realistic, varying from -8.5°C/km to 7°C/km, with a mean of -4.5°C/km. The precipitation lapse rate varied from -12 mm/km to 232 mm/km, with a mean of 17 mm/km. Basin wide annual precipitation averaged 683 mm over 2000-2010, while basin wide temperature averaged -0.29°C for the same period.

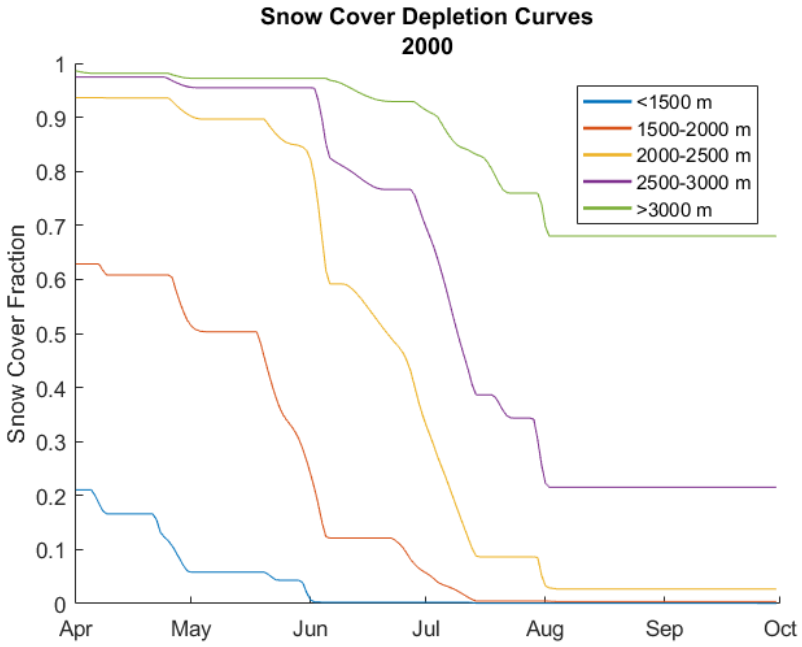

Figure 3: Snow cover fraction with melt season increases removed for the year 2000 (all elevation zones)

Before snow cover area data are used as input into the SRM model, any peaks in snow cover area during the melt season are removed. Following April 1st, any increases in SCA are set to the value prior to the increase for each elevation band, such that snow cover never increases in extent. This is done because snowfall events during the melt season are simulated by SRM from meteorological data rather than satellite observations. Removing melt-season snowfall events adjusts snowcover depletion curves to the pattern of melt for the base snowpack. The model computes runoff using the following equation:

$$Q_n = \sum_i (c_{Sin} a_{in} T_{in} SCA_{in} + c_{Rin} P_{in} RCA_{in}) (1 - k(x,y)_n) + Q_{n-1} k(x,y)_n \quad (3)$$

The runoff Q on day n is calculated from the individual contributions of snowmelt, rainfall, and recession from the previous day discharge. The rainfall and snowmelt contributions are summed over each elevation zone i. Snowmelt for each zone is calculated using the mean daily

temperature over the zone, T, the Degree Day Factor (DDF), a, and multiplying by the snow covered area, SCA to obtain melt volume. Rainfall runoff is calculated using the rainfall depth, P and multiplying by the rainfall contributing area RCA. Before the snowpack becomes ripe, rain on snow is assumed to become part of the snowpack and RCA is the zonal area excluding SCA. Once ripe, rain on snow contributes to runoff immediately, thus RCA no longer excludes SCA. Precipitation is partitioned into rain or snow based on the critical temperature parameter (not appearing in the above equation), which is set during calibration. If the zonal temperature is below the critical temperature, precipitation is determined to fall as snow and does not contribute immediately to runoff. Accumulated snow due to precipitation is tracked until positive temperatures release the stored water content to contribute to runoff. The runoff coefficients c_S and c_R account for losses due to evaporation and sublimation. The recession coefficient k, which expresses the decline in discharge during a period with no snowmelt or rainfall, transforms the daily influx of water into runoff. k is dependant on the previous day discharge (Equation 4).

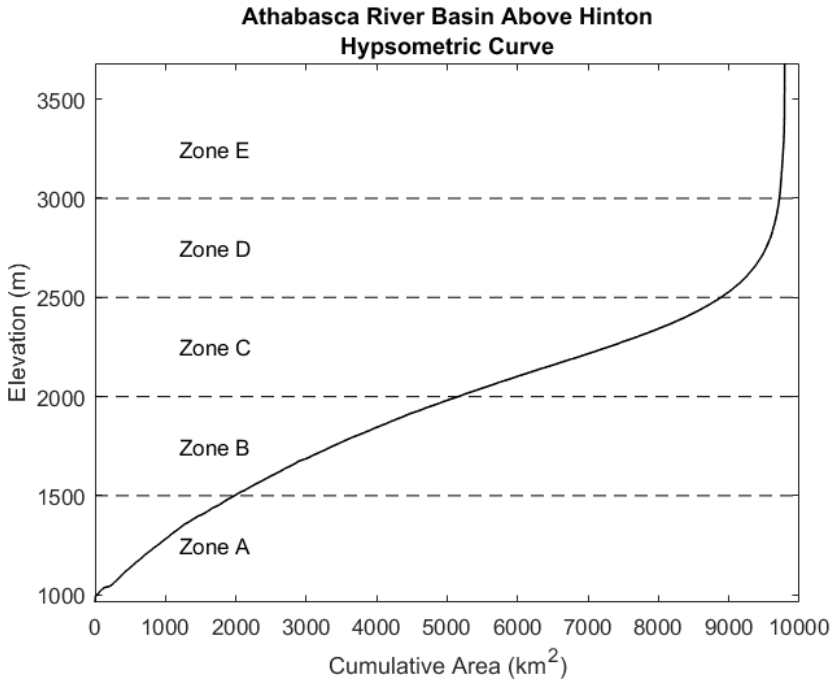

Figure 4: Hypsometric curve for study area with elevation bands

SRM handles runoff routing through the recession coefficient. The recession coefficient determines 'responsiveness' of the basin: how quickly the flow rises in response to rainfall or snowmelt, and how quickly flow recedes in their absence. The higher the recession coefficient, the less responsive the hydrograph will be. The basin response will vary depending on basin conditions. For example, groundwater has a much slower response than overland flow, thus during low flows when groundwater contributes a larger proportion of the flow, the basin would be expected to be less responsive. To account for the variation in the basin response, the recession coefficient is treated as a function of discharge:

$$k_n = \frac{Q_n}{Q_{n-1}} = xQ_{n-1}^{-y} \tag{4}$$

SRM allows for monthly, biweekly, or daily changes in the DDF for each elevation band to account for the seasonal and elevational variation in the DDF (Martinec et al., 2008). DDF values

may be determined through snow pillow or snow lysimeter measurements; an empirical relationship with snow density (Martinec, 1960); or based on energy-balance modelling. In the absence of physical measurements, the DDF may instead be calibrated (e.g., Panday et al., 2014) or chosen based on values from other studies in the same geographical area. As no data was available for calculation of the DDF in the study area, this parameter was determined through calibration. Three DDF approaches were examined: calibrating the DDF individually for each month, as is the standard approach in SRM; varying the DDF sinusoidally between maximum and minimum values on the summer and winter solstices, respectively (e.g., Anderson, 2006; Braun et al., 1993); and holding the DDF constant throughout the year, to examine the performance of a less realistic representation of melt. The model was run both with and without the inclusion of a separate DDF for glaciated areas. Glacier-covered area was taken to be the minimum observed SCA over the study period. The glacier DDF was scaled from the snow DDF for simplicity, as it is expected to follow a similar seasonal variation. Calibrating monthly DDF for glacier area resulted in only a minor improvement in model fit. The only spatial variation examined in these scenarios is in the glacier vs snow DDF (i.e. no zonal variation); though a comparison between the inclusion of the glacier DDF and calibrating zonal DDF values is included in the results.

Early in the melt season, melt at the snow surface may not immediately generate runoff. Surface melt will refreeze within the snowpack while subsurface temperatures remain below freezing, and even an isothermal snowpack can retain 2-10% of the snowpack weight as liquid water. Similarly, rain falling on an unripe snowpack may not immediately contribute to runoff. Once the snowpack is isothermal and its liquid holding capacity is satisfied, it is said to be ‘ripe’

and any additional melt or rain on the snow surface contributes to runoff. SRM accounts for rain on snow through the Rainfall Contributing Area (RCA) parameter, which assumes rain on snow does not contribute towards runoff until the snowpack is ripe. Prior to the snowpack becoming 'ripe', rain on snow is assumed to be absorbed by the snowpack and does not contribute to runoff until melt occurs. The retention of surface melt by the snowpack is not explicitly accounted for in SRM. The date at which the snowpack becomes ripe is set as a parameter to be calibrated. While the ripeness date is expected to vary spatially with the snowpack ripening later at higher elevations, a single ripeness data is used here to minimize parameters to be calibrated.

The critical temperature parameter is used to determine whether precipitation falls as rain or snow in each elevation zone. If the mean daily temperature for a zone exceeds the critical temperature, precipitation is classified as rain, and contributes immediately to runoff. Otherwise precipitation is classified as snow and is added to storage for that zone, only contributing to runoff once melt occurs. SCA is set to 100% when a zone has snow in storage such that snowmelt occurs over the entire elevation zone where there is snow in storage. Snow storage is only intended to capture short lived snowfall events during the melt season, with the use of remotely sensed imagery intended to capture the accumulated winter snowpack. As such, snow storage is only tracked between April 1st and October 31st.

Lag time was examined by comparing plots of hourly discharge for the Hinton stream gauge with hourly weather data from the Jasper Warden station. The lag between a rainfall or snowmelt event and a peak in runoff is unclear, as runoff tends to steadily increase over several days of warm temperatures or precipitation. Ideally, a peak in temperature would be followed

by a peak in runoff resulting from snowmelt, with the delay between the two being used to determine the lag time of the basin. However, only rarely is a sub-daily peak in runoff present that can be associated with melt from a single day, and these peaks are relatively small. A lag time of 28 hours appeared to give the best fit.

3.3.1 Markov Chain Monte Carlo (MCMC) methods

Calibration and parameter uncertainty analysis was performed using the Markov Chain Monte Carlo (MCMC) technique. Several MCMC based algorithms have been developed, all of which utilize a random walk to efficiently explore the parameter space (Smith and Marshall, 2008). The Metropolis-Hastings algorithm as described in Braswell et al. (2005) was utilized using code provided by Zobitz et al. (2011).

Parameter	Symbol
Critical Temperature (°C)	T_c
Runoff Coefficient (Snow)	c_S
Runoff Coefficient (Rain)	c_R
x (Recession Coefficient)	x
y (Recession Coefficient)	y
Snowpack Ripeness Date	RCA
DDF (cm °C^{-1} day^{-1})	a

Table 1: List of parameters determined by calibration. Multiple DDF values were calibrated for various model setups as described in Results section, (e.g. separate monthly DDF values, separate DDF values for snow vs glacial ice).

The MCMC algorithm utilizes the user's knowledge of the system being modeled through the prior distribution of model parameters. The prior distribution represents the probability of parameter values based on existing knowledge of the system. Typically, the prior distribution is assumed to be uniformly distributed between minimum and maximum allowable values (Zobitz et al., 2011). MCMC optimizes model fit by a randomly perturbing one parameter at a time within the range of allowable valuables until model fit reaches a maximum. During each

iteration, the new parameter value is accepted if model fit was improved. New parameter values with worse model fit are randomly accepted with an inverse relationship between the decrease in model fit and the probability of acceptance. This random allowance of worse model fits helps prevent convergence on local rather than global optima. A second technique used to ensure the global optimum is to initialize multiple chains at random starting points. The chain with the best model fit is selected as the starting point for a new chain, which is used to explore the parameter space around the global optimum. MCMC produces a set of accepted values that provides information about the posterior distribution. The distance by which each parameter is perturbed is adjusted each iteration to obtain a specified acceptance rate of new parameter values. As the chain progresses, the parameter perturbation distance is decreased as the random walk narrows in on an optimum.

The model was calibrated using observed runoff data for the years 2000 through 2002. These years displayed sufficient variability in meteorological and snow conditions to be representative of interannual variability for the basin. Following model calibration, the model was run for 2003 through 2010 to validate the applicability of calibrated model parameters outside of the calibration period. Parameter values were constrained to a realistic range based on the existing SRM literature and calibrated using the Monte Carlo Markov Chain (MCMC) method. Three Markov chains were initialized for each calibration run, with a final chain of 10,000 iterations being run starting from the best of the initial chains. Only parameter values from the final chain were accepted as part of the posterior distribution. Multiple calibrations were performed for each model set up to confirm they converged on the same optimum. The Nash Sutcliffe

Efficiency (NSE) was used as the cost function for the calibration. The parameter set with the best model fit (NSE) over the calibration period was treated as the 'definitive solution'.

Though the runoff coefficients were held constant throughout the year, in reality they would be expected to vary seasonally with evapotranspiration. The runoff coefficients for both rain and snow were selected through parameter calibration. As the calibration cannot distinguish the runoff coefficient for snow from the DDF, there would be little utility in allowing both to vary. Experiments incorporating monthly rainfall runoff coefficients showed only marginal improvement in model results, thus the rainfall runoff coefficient was held constant as well, as the inclusion of insensitive parameters in the calibration process acts to slow the search for the global optimum.

3.3.2 Evaluating Model Accuracy:

Model results were evaluated using the Nash Sutcliffe Efficiency (NSE) and percent bias. The NSE can range from -∞ to 1, with 1 indicating a perfect fit between model results and observations. NSE is given by:

$$NSE = 1 - \frac{\sum_{i=1}^{n}(Qo_i - Qm_i)^2}{\sum_{i=1}^{n}(Qo_i - \overline{Qo})^2} \quad (5)$$

Where Qo_i and Qm_i are the observed and modelled runoff values, respectively, and $\overline{Qo}$ is the mean of the observed runoff values over the modelled period. The percent bias is given by:

$$PBIAS = 100 \cdot \frac{\sum_{i=1}^{n}(Qm_i - Qo_i)}{\sum_{i=1}^{n} Qo_i} \quad (6)$$

3.4 Results and Discussion

3.4.1 Model Performance

Applying a spatially invariant DDF, all three temporal DDF approaches (constant, monthly, sinusoidal) gave comparable model fit (Table 2) over both the calibration and validation periods. PBIAS was negative for most years for the monthly and sinusoidal approaches, while being positive most years for the constant DDF approach. The year 2000 was overestimated with PBIAS greater than 10% for all approaches, experiencing the highest percentage runoff error of any year for the constant and sinusoidal approaches. Percentage error was below 10% for all other years except under the monthly approach, which experienced higher runoff error than the other approaches. All three approaches produced visually similar hydrographs; modelled discharge was unresponsive relative to observed flow, missing runoff peaks and troughs in favour of a smoothed hydrograph (Figure 6). The modelled hydrographs captured the seasonal runoff pattern well, allowing for high model fit despite missing much of the shorter-term variability in flow.

	Without Glacier DDF			With Glacier DDF		
	Constant	Sinusoidal	Monthly	Constant	Sinusoidal	Monthly
Calibration	0.887	0.885	0.886	0.924	0.944	0.932
Validation	0.828	0.846	0.844	0.819	0.874	0.880

Table 2: Calibration (2000-2002) and Validation (2003-2010) period NSE values for various DDF approaches

The inclusion of a separate DDF over glacier-covered areas resulted in a notable improvement in model fit for all three approaches over the calibration period (Figure 5). Validation period results for the sinusoidal and monthly approaches also displayed improvement, whereas the constant DDF approach did not. PBIAS was reduced over the calibration period for all approaches, but only the monthly approach displayed improvement over the validation period. Modeled hydrographs were more responsive, now capturing much of the short-term variability

in flow on top of the seasonal runoff pattern (Figure 6, Figure 7). While the non-glacier approach hydrographs had the appearance of an initial melt pulse followed by slow flow recession, the separate DDF more accurately captured individual runoff peaks.

Results compared favorably to those of Fitzharris and Sirguey (2014), with equal or greater model fit (NSE) for most years. Parameter value choices in Fitzharris and Sirguey (2014) differed significantly from this thesis with the DDF being calculated from albedo on a pixel by pixel basis for a fully distributed implementation of SRM, along with a recession coefficient which was much less sensitive at low flows while more sensitive at high flows. Results from their study differed in several aspects from the results in this thesis, with different errors in runoff being encountered. Some errors were consistent between Fitzharris and Sirguey (2014) and results presented in this thesis, such as a mixed runoff peak in 2010, likely a heavy rainfall event missed in the meteorological data.

The range of calibration and validation period model fits for each DDF approach was examined when accounting for parameter uncertainty (Figure 5). The constant DDF approach did not produce any parameter sets with validation period NSE values over .854, whereas 50% of sinusoidal and 26% of monthly approach parameter sets had validation period model fit over .854. Model fit and hydrograph appearance was similar between monthly and sinusoidal DDF approaches, although the sinusoidal approach displayed the most consistent relationship between calibration and validation period model fit. The sinusoidal DDF captured the seasonal cycle of the DDF while having less parameters to calibrate than the monthly approach. Calibrated monthly DDF values tended to follow a sinusoidal pattern, increasing toward a maximum in July. This is consistent with energy-balance model calculations which have shown

seasonal variation in the DDF to follow a sinusoidal pattern (Anderson, 2006). The importance of accounting for the seasonal cycle of the DDF is exhibited by comparing it with the constant DDF approach, which, even with the inclusion of the glacial component, stands out against the other approaches with its lesser model fit (Table 2).

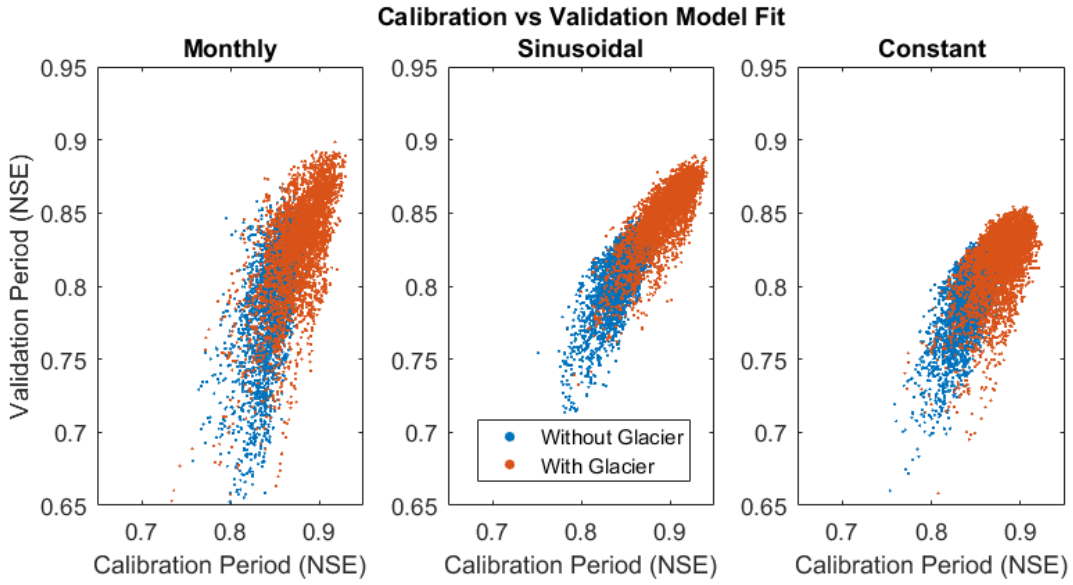

Figure 5: Calibration vs validation model fit for various approaches to the DDF

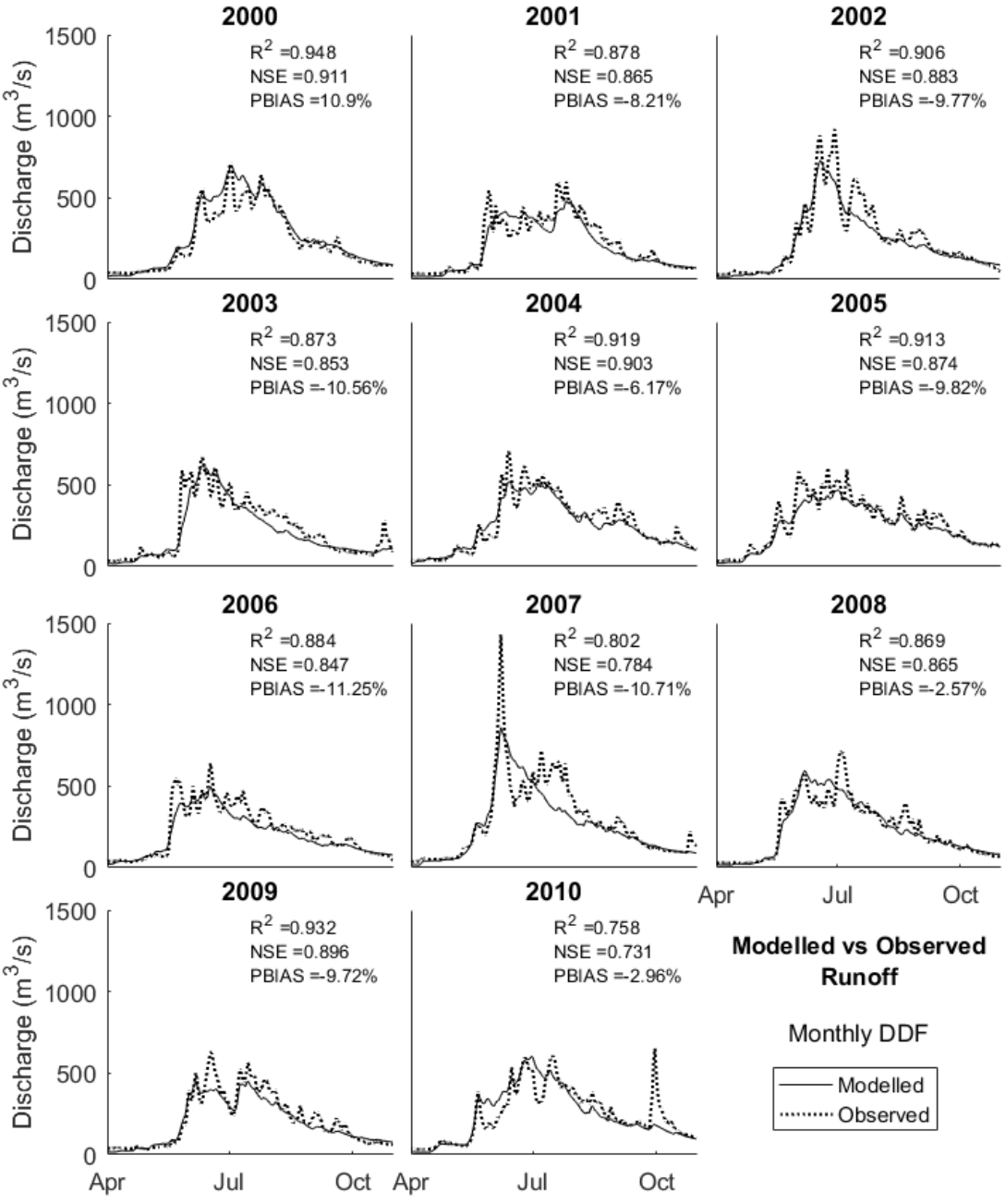

Figure 6: Simulated runoff for 2000-2010 using the monthly DDF approach without a separate DDF for glaciated areas

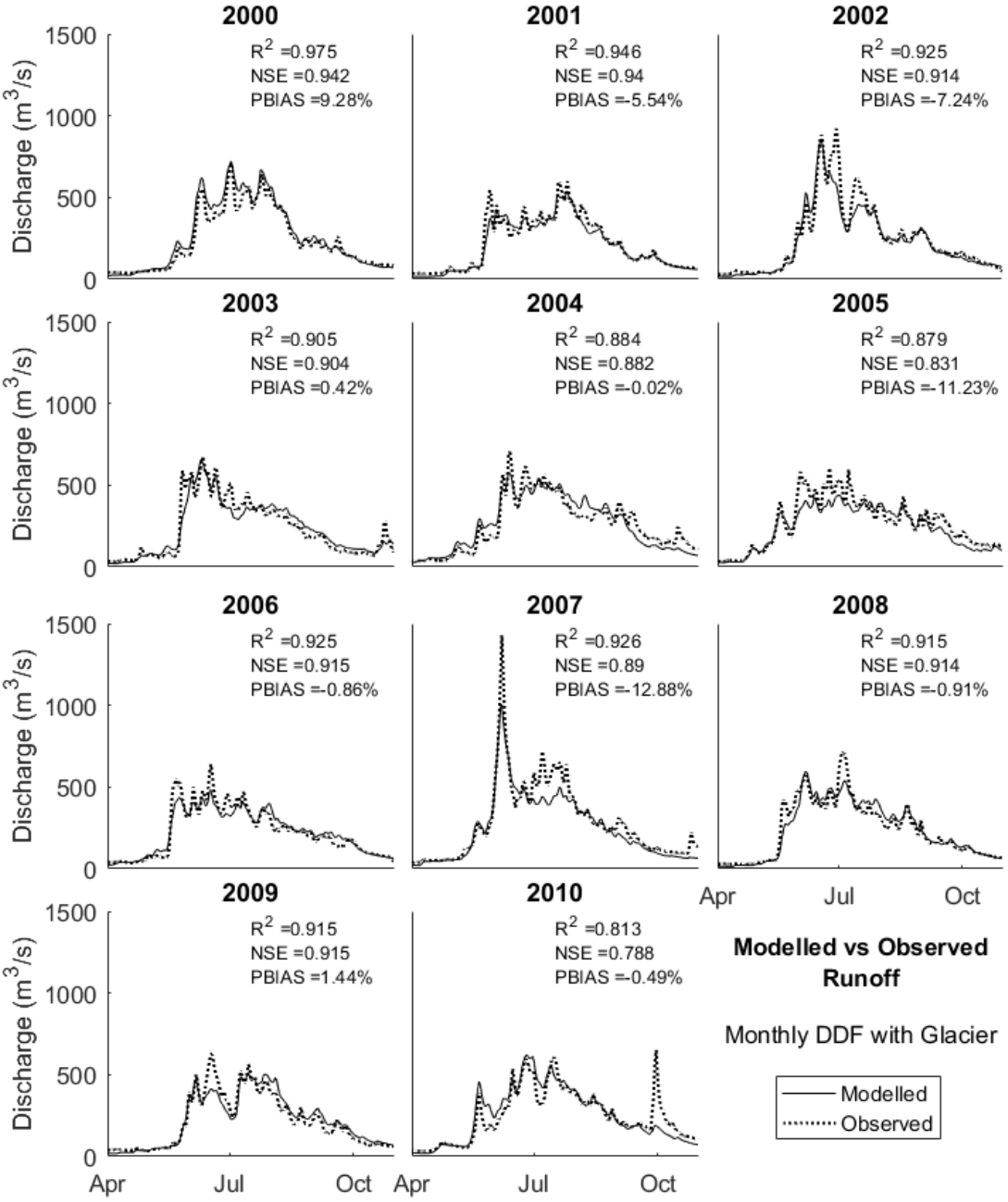

Figure 7: Simulated runoff for 2000-2010 using the monthly DDF approach with a separate DDF for glaciated areas

3.4.2 Parameter Distributions and Sensitivity

The posterior distributions of the most sensitive parameters were well constrained. The recession coefficients had the narrowest posterior distributions, as small perturbations to these parameters have a substantial impact on the hydrograph. The recession coefficient parameters were highly interdependent, having a linear relationship between 'x' and 'y' values which provide equally good model fit. While higher 'y' values increase hydrograph responsiveness at higher flows relative to lower flows, higher 'x' values increase responsiveness across all flows. This linear relationship corresponds to 'x' and 'y' parameter combinations which produce similar responsiveness over the midrange of flows, with differences in responsiveness between parameter sets primarily occurring at the highest and lowest modelled flows.

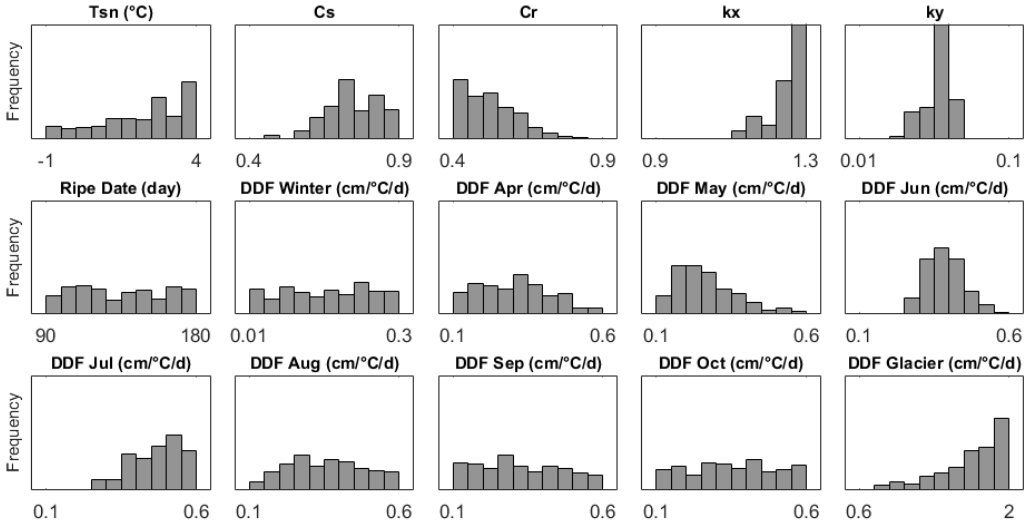

Figure 8: Posterior distributions of model parameters for monthly DDF with glacier approach. Critical temperature (Tsn), snowmelt runoff coefficient (Cs), rainfall runoff coefficient (Cr), recession coefficient parameters (x and y), date of snowpack ripeness in days since start of calendar year (Ripe Date), the DDF over the November-March (DDF Winter), and DDF for individual months from April through to October.

The runoff coefficients were both moderately constrained, with the rainfall runoff coefficient constrained to the lower end of its range and the snowmelt runoff coefficient constrained to

the middle to upper end of its range. For the monthly DDF with glacier approach, DDF values at which the posterior distribution peak occurred increased from May through to July, being constrained to the lower end of its range in May, the middle of its range in June, and the high end of its range in July. Monthly DDF values were poorly constrained outside of May to July, as the lower contribution of melt to runoff in these months renders model fit less sensitive to perturbations in the DDF. The late June maximum of the sinusoidal approach places its seasonal progression slightly ahead of the monthly approach. Maximum DDF values tended to be lower for the sinusoidal approach than for the monthly approach. The glacier DDF peaked in likelihood at the upper limit of its range, indicating higher glacier DDF values would provide improved model fit. The glacier DDF was limited to 2 cm/°C/day, the maximum of the observed and calculated DDF values of the studies summarized by Hock (2003).

Critical temperature displayed a broad posterior distribution with a preference towards higher temperatures. Critical temperature parameter values were constrained by the upper parameter limit of 4°C, particularly in the case of the sinusoidal DDF. Higher critical temperatures were found to decrease runoff earlier in the year in April and May, while flows during the warmer months (July, August) remained unchanged. As SRM assumes snowfall on the seasonal snowpack becomes part of the snowpack, higher critical temperature values cause precipitation that would otherwise be considered rain and immediately contribute to runoff to instead be stored as snow. This gives the critical temperature parameter a similar effect as the ripeness parameter, which assumes rain on snow prior to the snowpack becoming ripe becomes part of the snowpack. Once precipitation is part of the seasonal snowpack, it is effectively lost to runoff, as the seasonal snowpack is set by snow cover imagery and would contribute the same

amount of melt to runoff regardless of whether the model determines precipitation to become part of it. Both critical temperature and ripeness parameters act to reduce runoff early in the year when SCA is high. However, the ripeness parameter has a uniform posterior distribution. Varying the ripeness parameter over the allowable range of values while the critical temperature was high (4°C) produced negligible change to the hydrograph, with NSE decreasing by up to .002. Dropping the critical temperature to 0°C reduced calibration period NSE from .932 to .906 but resulted in much higher sensitivity to the ripeness parameter. With the lower critical temperature, pushing the ripeness parameter late in the year produced a similar effect to the high critical temperature, reducing early season flows.

3.4.3 Model Bias

The model failed to capture certain aspects of observed hydrographs regardless of DDF approach. Winter flows were underestimated in every year for most model configurations (Figure 9). The sub-freezing temperatures experienced by the Upper Athabasca Basin over the winter months result in little meltwater production or rainfall to maintain flows throughout the winter. Without meltwater or rainfall, the modelled hydrograph declines in accordance with the recession coefficient, receding below the observed flow. The recession coefficient is a simplified representation of runoff routing and baseflow in a basin, and its limitations may be responsible for underestimated winter flows. The recession coefficient assumes the basin will be more responsive at higher flows when overland flow dominates, and less responsive at lower flows when ground water contributes a larger proportion of runoff. The recession coefficient must be responsive enough at low flows to capture the initial rise in discharge with the onset of Spring melt, while not being so responsive that rapid flow recession occurs in the Fall as temperatures

descend below freezing. A compromise between the quick response of runoff in the Spring and slow recession through the Winter is necessary due to the set relationship between flow and basin response. A more realistic runoff routing routine which separates the baseflow from overland flow may improve model results in this regard.

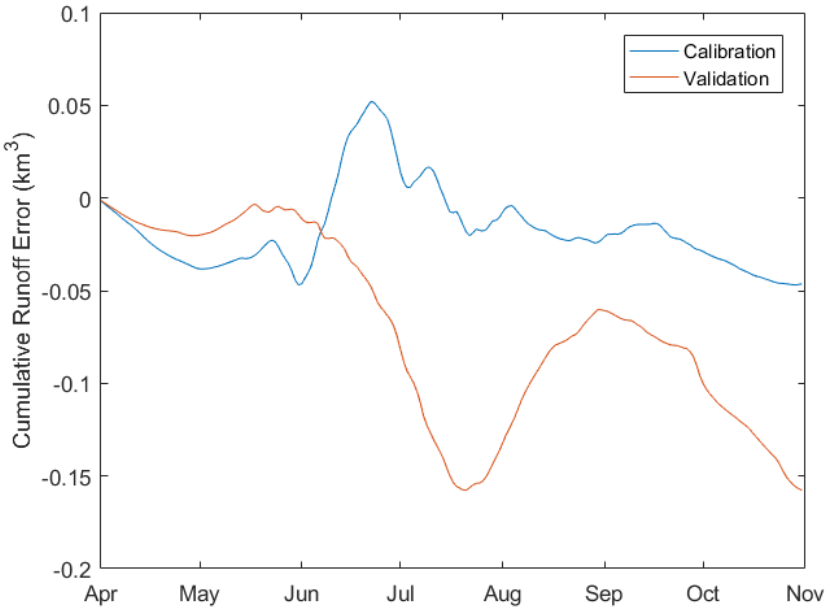

Figure 9: Cumulative model error averaged over calibration and validation periods for the monthly DDF model with separate glacier DDF

June and July flows were underestimated in most years over the validation period for all DDF approaches, as well as for the calibration period for the sinusoidal approach. Several notable runoff peaks are missed or underestimated during these months. The most significant missed runoff peaks occur coincident with SCA reaching its minimum in June (2009) or July (2002,2007,2008). Flow underestimation associated with below average snow cover also occurred in June 2005 and 2006. Flow overestimation occurred in 2000 and 2010, both years with above average snow cover in June and July.

The MODIS snow cover product has been found to underestimate snow cover (Kult et al., 2014), particularly when the snow cover fraction is below 20% (Dery et al., 2005). A persistent bias would be corrected for through calibration of the DDF or runoff coefficient, but greater underestimation at lower snow cover fraction would lead to flow underestimation when SCA is small. This SCA underestimation may be responsible for the missed June and July runoff peaks. Additional SCA underestimation may stem from the methodology used to derive the snow cover depletion curves. All increases in SCA after April 1st are removed so only the seasonal snowpack is captured by the depletion curve. If any erroneously low SCA occurred, this method would have the effect of locking in the low value. SRM was run without removing melt season increases in SCA to assess whether this methodology was contributing to model error. Inclusion of melt season increases in SCA had negligible effect on results except for a minor reduction in flow underestimation for the missed June runoff peak in 2009.

SCA underestimation may also contribute to the glacier model tendency to overestimate August runoff. As the model calibration selects a higher DDF to compensate for underestimated SCA, this DDF generates excess melt later in the season when the MODIS SCA input is constant despite actual SCA declining as the remaining patchy snow cover melts. However, SCA underestimation does not fully explain August flow overestimation, as this bias is present in the monthly DDF approach where adjusted monthly DDF values could correct for model bias. August flow overestimation is only present in the monthly DDF validation period, indicating the model is failing to account for different hydrological conditions between the calibration and validation periods. Late-season flow overestimation is particularly prevalent in the constant DDF approach. Whereas a declining DDF reduced model overestimation in August and

September in the other approaches, the constant DDF approach exhibits consistently overestimated flows through to November.

Glacier area was approximately 320 km^2 when calculated from GLIMS glacier outlines, almost twice that of the 180 km^2 MODIS SCA minimum. This underestimation of glacier covered area may explain the high glacier DDF selected for by the calibration process, as the DDF compensates for the low glacier covered area. However, using the GLIMS glacier cover estimate also did not improve model results, with flow overestimation occurring from July onwards for several years. This is consistent with the underestimation of patchy SCA in the MODIS data, as correcting glacier area using GLIMS glacier covered area without correcting SCA would require a higher DDF to correct for underestimated SCA when snow cover is patchy, which would then overestimate melt once SCA declines.

3.4.4 Interannual Variability and the Importance of the Glacial DDF

Though glaciers represent only 3% of the basin area, they provide a disproportionate fraction of late summer runoff. Glaciated areas represented over half of the basin cryosphere area by July 18th on average (2000-2010), and as early as June 26th. The increased model fit of the glacier approach is associated with the increased responsiveness of the hydrograph. The greater summer melt at low SCA provided by the glacier component is essential to this increased responsiveness, as a more responsive recession coefficient without sufficient summer melt would lead to rapid flow recession and vastly underestimated late summer flows. The calibration process does not select for a higher summer DDF for the non-glacier model due to interannual variability in melt conditions. During a low snow year, glacial ice will be exposed earlier and the effective average DDF of the basin will be higher than during a year with a

longer lasting snowpack. Because of this interannual variability in melt conditions, utilizing a basin wide DDF will result in substantial melt volume error, with the largest error occurring in late summer when the difference in DDF between snow and ice has the largest impact. The non-glacier model calibration reduces this error and consequential poor model fit by reducing late summer melt volume, instead capturing the seasonal flow pattern using a large initial pulse of meltwater and accompanying slow runoff recession.

The inability of the non-glacier model to capture interannual variability in melt conditions is illustrated by the increase in model responsiveness when calibrated for individual years. Calibrating the non-glacier model using individual years resulted in higher late summer DDF values and more responsive hydrographs for 2000 and 2001. The hydrograph remained unresponsive for 2002 due to the monthly resolution of the DDF; when calibrated using biweekly DDF values 2002 also displayed increased responsiveness more similar to the glacier model (Figure 10). Similar recession coefficient parameter values are obtained between individually calibrated years, with the primary difference in parameters sets being DDF values. As the non-glacier model is able to obtain high model fit for individually calibrated years with the primary difference in parameter values between years being DDF values, interannual variation in the DDF appears to drive the lower model fit and unresponsive hydrograph found when the model is calibrated over multiple years.

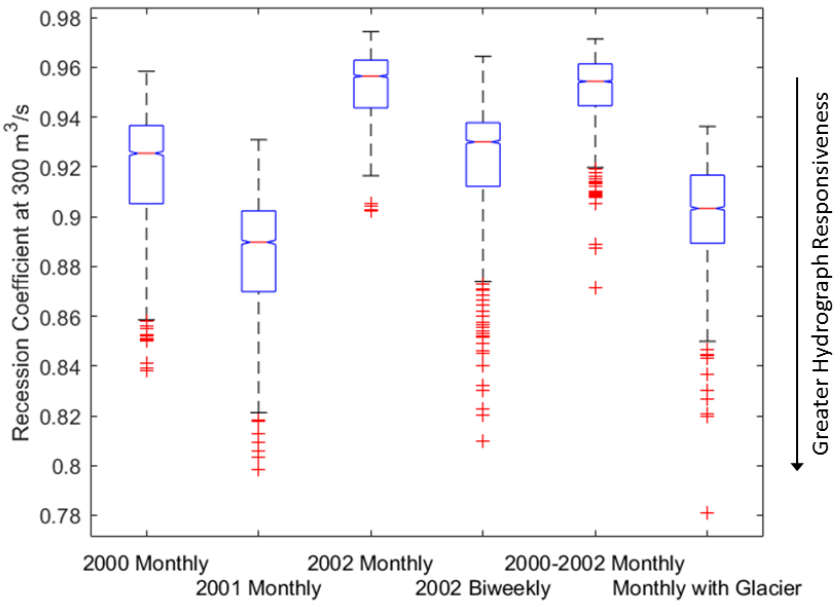

Figure 10: Recession coefficient at 300 m^3/s (close to the median annual discharge) from all parameter sets when calibrating one year at a time for the monthly DDF approach with no glacier for 2000-2002, using the biweekly DDF approach for 2002, using all three calibration years for the monthly no glacier approach, and using all three calibration years for the monthly with glacier DDF approach. The red lines represent the median parameter values, with the blue boxes spanning from the 25^{th} to 75^{th} percentiles. Red plus signs show outliers (>2.7 standard deviations from median), with the whiskers showing the most extreme parameter values not considered outliers.

The necessity of multiple calibration years was assessed for the glacier DDF model by performing single-year calibrations of the model (Table 3). Single-year calibrations of the monthly DDF with glacier approach produced improved results over their corresponding non-glacier approach calibrations, as the glacier DDF inclusion allows for improved timing of the seasonal DDF increase over what the monthly resolution permits. However, validation period model fit shows only slight improvement over the non-glacier model, as parameter values are specific to the calibration year. Higher monthly DDF values may compensate for a lower glacier DDF, as the glacier DDF is not needed for interannual variability when calibrated for a single year. Farther calibration period specific parameter values may stem from monthly DDF values

which compensate for model bias specific to that year. Calibration over multiple years of varying melt conditions is necessary to constrain parameters to more robust values. Unlike the monthly approach, single-year calibration using the sinusoidal approach produced validation period results of similar quality to using all three calibration years. The model is less able to adapt to year specific melt conditions when the DDF is constrained to a sinusoidal pattern rather than freely varying monthly values. Constraining the DDF to a realistic seasonal progression produced parameter sets which were more likely to be applicable outside of their calibration period. These findings confirm that constraining the model to more realistic representations of the physical processes (with the glacier component and sinusoidal DDF pattern) improves the robustness of the model outside of the calibration period.

Calibration Period	DDF Method	2000	2001	2002	Validation (2003-2010)
2000-2002	Monthly	0.911	0.865	0.883	0.844
2000-2002	Monthly with Glacier	0.942	0.940	0.914	0.880
2000	Monthly	0.966	0.708	0.709	0.620
2001	Monthly	0.771	0.946	0.775	0.775
2002	Monthly	0.477	0.811	0.918	0.757
2002	Biweekly	0.231	0.859	0.949	0.762
2000	Sin with Glacier	0.967	0.932	0.897	0.867
2001	Sin with Glacier	0.951	0.961	0.861	0.870
2002	Sin with Glacier	0.915	0.917	0.936	0.907
2000	Monthly with Glacier	0.974	0.804	0.831	0.736
2001	Monthly with Glacier	0.934	0.953	0.854	0.849
2002	Monthly with Glacier	0.864	0.829	0.938	0.726

Table 3: Model Fit (NSE) for individual calibration years and averaged over the validation period for various DDF approaches, comparing calibration using a single year with calibration using the whole 2000-2002 calibration period.

SRM studies typically vary the DDF independently for each elevation band. Several model runs were performed utilizing this zonal approach for comparison with the glacier model. The zonal DDF approach generated a modest improvement in calibration period model fit over the glacier DDF model (NSE of .953 for zonal DDF vs .932 for glacier DDF), but no improvement over the

validation period. The zonal DDF model produces higher flows in June and early July and lower flows in the later months, resulting in better model fit in some years (2002, 2004, 2005, 2008) where early melt season underestimation and late melt season overestimation were issues. Other years with those same issues (2006, 2007, 2009) experienced lower model fit due to the timing of the change in flow being too early (e.g., the zonal model overestimates flow just prior to the missed June runoff peak in 2009). Applying a higher DDF to the entire snowpack above 2500 m as opposed to just glacier area provides a similar effect to correcting underestimated snow cover: there is increased snowmelt runoff around the time of year when SCA is bottoming out due to a higher DDF being applied over the upper elevation bands. This higher DDF has little impact while snow cover is high and melt volume originates primarily from the lower elevation bands but has a larger effect on the hydrograph when the lower elevation snow cover is depleted and snowmelt is dominated by this higher DDF. As snow cover is expected to be preferentially underestimated when snow cover fraction is low, corrected SCA would similarly increase runoff when SCA is bottoming out and runoff is dominated by the higher elevations.

3.5 Conclusions

This study applied the Snowmelt Runoff Model (SRM) with remotely sensed snow cover information to simulate runoff for the Upper Athabasca River Basin at Hinton over the 2000-2010 period. The results demonstrated that both the zonal and glacial DDF approaches performed well in replicating the observed streamflow in the calibration and validation periods. The inclusion of a separate DDF for glaciers or for the higher elevation bands (effectively accounting for the higher DDF associated with glacial ice) was found to be essential to capturing

interannual variability in melt conditions. While a spatially invariant DDF performed well when calibrated for a single year, it performed poorly when applied to years with differing snow conditions. The addition of the glacier DDF improved model fit when the model was applied over multiple years with a range of snow conditions. Though the glacier model performed no better than the more typically applied zonal formulation of SRM, results indicate the higher DDF for glacial ice could explain much of the elevation dependence of the DDF. These results stress the importance of accounting for the higher melt factor of glacial ice, either explicitly or through a zonal DDF. Future work could investigate setting the DDF proportional to albedo, which could account for both temporal and spatial variation in the DDF. Differences in the DDF between forested (below ~2200 m) and alpine areas could also be investigated.

Scaling the glacial DDF from the snow DDF was found to provide comparable results to calibrating each separately, as both follow a similar seasonal pattern. The seasonal progression in the melt factor was found to be accurately captured by sinusoidally varying the DDF between a summer maximum and winter minimum. Constraining the DDF to a sinusoidal pattern generated more reliable results over the validation period than freely varying the DDF on a monthly basis. While SRM benefits from its simplicity and few required input variables, this study demonstrated that incorporating some process understanding about hydrological processes (such as glacial melt) could be advantageous to the robustness of model results under varying hydrological conditions.

References

Abudu, S., Sheng, Z. ping, Cui, C. liang, Saydi, M., Sabzi, H. Z., & King, J. P. (2016). Integration of aspect and slope in snowmelt runoff modeling in a mountain watershed. *Water Science and Engineering*, *9*(4), 265–273.

Anderson, E. (2006). Snow Accumulation and Ablation Model–SNOW-17. *Online Documentation*, 1–61.

Arnell, N. W. (1999). Climate change and global water resources. *Global Environmental Change*, *9*(SUPPL.), 31–49. https://doi.org/10.1016/S0959-3780(99)00017-5

Barnett, T. P., Adam, J. C., & Lettenmaier, D. P. (2005). Potential impacts of a warming climate on water availability in snow-dominated regions. *Nature*, *438*(7066), 303–309.

Beven, K., & Freer, J. (2001). Hydrology Equifinality, data assimilation, and uncertainty estimation in mechanistic modelling of complex environmental systems using the GLUE methodology. *Journal of Hydrology*, *249*, 11–29.

Bolch, Tobias, 2008. GLIMS Glacier Database. Boulder, CO. National Snow and Ice Data Center.

Braswell, B. H., Sacks, W. J., Linder, E., & Schimel, D. S. (2005). Estimating diurnal to annual ecosystem parameters by synthesis of a carbon flux model with eddy covariance net ecosystem exchange observations. *Global Change Biology*, *11*, 335–355.

EDW Working Group (2015). Elevation-dependent warming in mountain regions of the world. *Nature Clim. Change*, *5*(5), 424–430.

Déry, S. J., Salomonson, V. V., Stieglitz, M., Hall, D. K., & Appel, I. (2005). An approach to using snow areal depletion curves inferred from MODIS and its application to land surface modelling in Alaska. *Hydrological Processes*, *19*(14), 2755–2774.

Faurès, J. M., Goodrich, D. C., Woolhiser, D. A., & Sorooshian, S. (1995). Impact of small-scale spatial rainfall variability on runoff modeling. *Journal of Hydrology*, *173*(1–4), 309–326.

Feiccabrino, J., Graff, W., Lundberg, A., Sandström, N., & Gustafsson, D. (2015). Meteorological Knowledge Useful for the Improvement of Snow Rain Separation in Surface Based Models. *Hydrology*, *2*(4), 266–288.

Ferguson, R. I. (1999). Snowmelt runoff models. *Progress in Physical Geography*, *23*, 205–227.

Fitzharris B. & Sirguey P. (2014). Building a Platform for Snowmelt Runoff Modelling in the Athabasca River Basin, *Unpublished Report*

Georgievsky, M. V. (2009). Application of the Snowmelt Runoff model in the Kuban river basin using MODIS satellite images. *Environmental Research Letters*, *4*(4), 45017.

Hall, D. K., Riggs, G. a., Salomonson, V. V., DiGirolamo, N. E., & Bayr, K. J. (2002). MODIS snow-cover products. *Remote Sensing of Environment*, *83*(1–2), 181–194.

Hock, R. (2003). Temperature index melt modelling in mountain areas. *Journal of Hydrology*, *282*(1–4), 104–115.

Hock, R. (2005). Glacier melt: a review of processes and their modelling. *Progress in Physical Geography*, *29*(3), 362–391.

Hutchinson, M. F., McKenney, D. W., Lawrence, K., Pedlar, J. H., Hopkinson, R. F., Milewska, E., & Papadapol, P. (2009). Development and Testing of Canada-Wide Interpolated Spatial Models of Daily Minimum – Maximum Temperature and Precipitation for 1961 – 2003, 725–741.

Kult, J., Choi, W., & Choi, J. (2014). Sensitivity of the Snowmelt Runoff Model to snow covered area and temperature inputs. *Applied Geography*, *55*, 30–38.

Li, X., & Williams, M. W. (2008). Snowmelt runoff modelling in an arid mountain watershed, Tarim Basin, China. *Hydrological Processes*, *22*, 3931–3940.

Liu, Y., & Gupta, H. V. (2007). Uncertainty in hydrologic modeling: Toward an integrated data assimilation framework. *Water Resources Research*, *43*(7), 1–18.

Ma, Y., Huang, Y., Chen, X., Li, Y., & Bao, A. (2013). Modelling snowmelt runoff under climate change scenarios in an ungauged mountainous watershed, Northwest China. *Mathematical Problems in Engineering*.

Martinec, J., Rango, a, & Roberts, R. (2008). Snowmelt runoff model (SRM) user's manual. *Agricultural Experiment Station Special Report 100*.

Panday, P. K., Williams, C. a., Frey, K. E., & Brown, M. E. (2014). Application and evaluation of a snowmelt runoff model in the Tamor River basin, Eastern Himalaya using a Markov Chain Monte Carlo (MCMC) data assimilation approach. *Hydrological Processes*, *28*(21), 5337–5353.

Rango, A., & Martinec, J. (1995). Revisiting the degree-day method for snowmelt computations. *Water Resources Bulletin*, *31*(4), 657–669.

Raup, B.H.; A. Racoviteanu; S.J.S. Khalsa; C. Helm; R. Armstrong; Y. Arnaud (2007). "The GLIMS Geospatial Glacier Database: a New Tool for Studying Glacier Change". Global and Planetary Change 56:101--110.

Rood, S. B., Pan, J., Gill, K. M., Franks, C. G., Samuelson, G. M., & Shepherd, A. (2008). Declining summer flows of Rocky Mountain rivers: Changing seasonal hydrology and probable impacts on floodplain forests. *Journal of Hydrology*, *349*, 397–410.

Schindler, D. W., & Donahue, W. F. (2006). An impending water crisis in Canada's western prairie provinces. *Proceedings of the National Academy of Sciences of the United States of America*, *103*(19), 7210–6.

Smith, T. J., & Marshall, L. A. (2008). Bayesian methods in hydrologic modeling : A study of recent advancements in Markov chain Monte Carlo techniques, *44*(July), 1–9.

Tahir, A. A., Chevallier, P., Arnaud, Y., Neppel, L., & Ahmad, B. (2011). Modeling snowmelt-runoff under climate scenarios in the Hunza River basin, Karakoram Range, Northern Pakistan. *Journal of Hydrology*, *409*(1–2), 104–117.

Vafakhah, M., Nouri, A., & Alavipanah, S. K. (2014). Snowmelt-runoff estimation using radiation SRM model in Taleghan watershed. *Environmental Earth Sciences*, *73*, 993–1003.

Woo, M. K., & Giesbrecht, M. A. (2000). Simulation of snowmelt in a subarctic spruce woodland: 1. Tree model. *Water Resources Research*, *36*(8), 2275–2285.

Zobitz, J. M., Desai, A. R., Moore, D. J. P., & Chadwick, M. A. (2011). A primer for data assimilation with ecological models using Markov Chain Monte Carlo (MCMC). *Oecolgia*, 599–611.

4 Chapter 4: Projecting Runoff in the Upper Athabasca River for a Warming Climate

Abstract

Warming temperatures have shifted runoff in snowmelt dominated catchments, resulting in earlier spring peak flows and lower summer runoff. Climate change projections show continued warming which will intensify current runoff trends. Quantifying these changes will assist in managing water resources and preparing for a new seasonal distribution of runoff. The Snowmelt Runoff Model (SRM) was utilized in assessing the effects of climate change on the Upper Athabasca River at Hinton. Four climate change scenarios were examined for the 2070-2080 period representing uncertainty in climate change projections. All scenarios resulted in substantial increases in May flow and corresponding decrease in May snow cover fraction. Winter months are projected to experience small increases in flow, though these increases represent sizable percentage increases in flow (5-139%, depending on month and climate change scenario). Results were consistent with previous modelling studies of the region and historical trends, and there was little variation in modelled trends when accounting for parameter uncertainty. These results show SRM is a useful model for climate projections with few, widely available input variables and relatively simple operation.

4.1 Introduction

The Western Prairie Provinces of Canada are semi-arid, relying on rivers and groundwater originating from the Rocky Mountains to supply their water requirements (Schindler and Donahue, 2006). The Athabasca River is one such large and undammed river in Alberta, originating from Athabasca Glacier on the eastern slopes of the Canadian Rockies and flowing northeastward to Lake Athabasca. Industrial development led by petroleum production around the Athabasca Oil Sands has fueled population growth in the prairie province of Alberta. Water from the Athabasca River is utilized for oil extraction from the Athabasca Oil Sands, downstream from Fort McMurray in the lower portion of the basin. The river is utilized for municipal, agricultural, and other industrial uses, and is representative of the many other rivers originating in the Rocky Mountains which supply the Canadian Prairies with water.

Like most regions at similarly high latitudes, runoff in the Canadian Prairies is dominated by snowmelt (Barnett et al., 2005); and wherever snowmelt contributes significantly to streamflow, the seasonal distribution of runoff is heavily influenced by temperature (Adam et al., 2009). Snow plays a significant role in the hydrological cycle, storing water through the winter and releasing it in the spring as melt. Increasing temperatures in snowmelt dominated basins will shift peak flows earlier in the year, decreasing summer flows while increasing winter flow. Glacier presence is of particular importance for maintaining late summer flows, with historical decreasing trends in August flows observed in glaciated basins throughout British Columbia associated with a retreat in glacier area (Stahl and Moore, 2006). Trend analysis of observed flows over the past century for nival rivers throughout the Rocky Mountains confirm the shift towards earlier peak flows and reduced summer runoff is already occurring in

association with warming winter and spring temperatures (Rood et al., 2008). Bawden et al. (2014) examined flow trends for hydrometric stations across the Athabasca River basin between 1966 and 2010, finding most stations in the basin experienced strong decreases in annual and summer month flows. The Athabasca River Basin (ARB) did not experience noteworthy warm season (March- October) temperature trends between 1976 and 2010, but negative trends in precipitation were observed basin wide, particularly in the upper and mid-ARB (Bawden et al., 2014). O'Neil et al. (2016a) found increasing temperature trends across Western Canada between 1950 and 2010, with the strongest increase in winter. Decreased precipitation was noted in the cold season, while precipitation increased in the warm season.

Regional climate models projected 1.5 to 2.5°C warming of annual mean daily maximum temperature and 3°C warming of annual mean daily minimum temperature over 2041-2070 relative to 1971-2000 (O'Neil et al., 2016b). Precipitation is also expected to increase across Western Canada, though there is greater spatial variability in projected precipitation changes and reduced model agreement relative to temperature projections (O'Neil et al., 2016b). Consistent with historical trends, winter is expected to undergo the strongest warming, while summer undergoes a weaker warming trend than other seasons. With snowmelt being the primary source of runoff most regions north of 45°N (Barnett, 2005), warming temperatures due to climate change will shift runoff timing over a substantial portion of the globe. The resulting decline in summer flows will be problematic given water usage is highest in summer due to withdrawals for irrigation and municipal water use (Schindler and Donahue, 2006). Dibike et al. (2018) investigated the snow response to climate change in the Athabasca basin using the VIC hydrological model, projecting reduced SWE throughout the Athabasca River

Basin, particularly in the upper basin, and earlier occurrence of max SWE. Glacier areas in the Canadian Rockies are also expected to decline by up to 90% by the end of the century, with the maximum rate of decline occurring between 2020 and 2040 (Clarke et al., 2015).

Modelling future runoff is a useful exercise for planning and water resource management. Rango et al. (2008) examined multiple climate change scenarios with Snowmelt Runoff Model (SRM) for the glacierized Illecillewaet basin in British Columbia, Canada. While accounting for reduced snow cover area, this study did not account for reduced glacier cover. Nolin et al., (2010) simulated the effects of a warming climate on glacial runoff for a small basin in the Pacific Northwest of the United States, with results showing reduced runoff as shrinking glacier cover more than compensated for increased melt from warmer temperatures. Tahir et al. (2011) and Ma et al. (2013) utilized SRM in examining the hydrological impacts of climate change on basins in Northern Pakistan and North Western China, respectively. Many SRM climate studies prescribe a set change in cryosphere area or utilize a range of cryosphere change scenarios (Nolin et al., 2010; Tahir et al., 2011; Ma et al., 2013).

The objective of this study is to project future runoff in the Upper Athabasca River Basin using the SRM. Following this introductory section, the study watershed is described in section 2. Description of the hydro-climatic data used for setting up of the hydrologic model is provided in section 3 followed by description of the methods used for hydrologic modelling and analysis in section 4. The modeling results are presented in section 5 followed by the conclusion of the study in Section 6.

4.2 The Study Area

The focus of this study is the Upper Athabasca River Basin (UARB) above Hinton (Figure 11). The 9760 km^2 study basin is almost entirely located within the mountainous topography of the Rocky Mountains, with elevations ranging from 960 m asl to 3740 m asl. Located between 52°07' N and 53°29' N in latitude, the basin experiences a subarctic climate with coniferous forest up to 2200 m elevation. The mean annual precipitation in the basin is around 638 mm with 47% falling as snow. The mean monthly temperature in the basin range from around -10^{o}C in January to over 11^{o}C in July with significant interannual variability. Runoff is snowmelt dominated, with low winter flows followed by the onset of snowmelt in Late April or May. Flow typically peaks in June or July before gradually declining back to winter low flow. Glaciers are present in the upper elevations, with glacial ice covering 3% of the basin area.

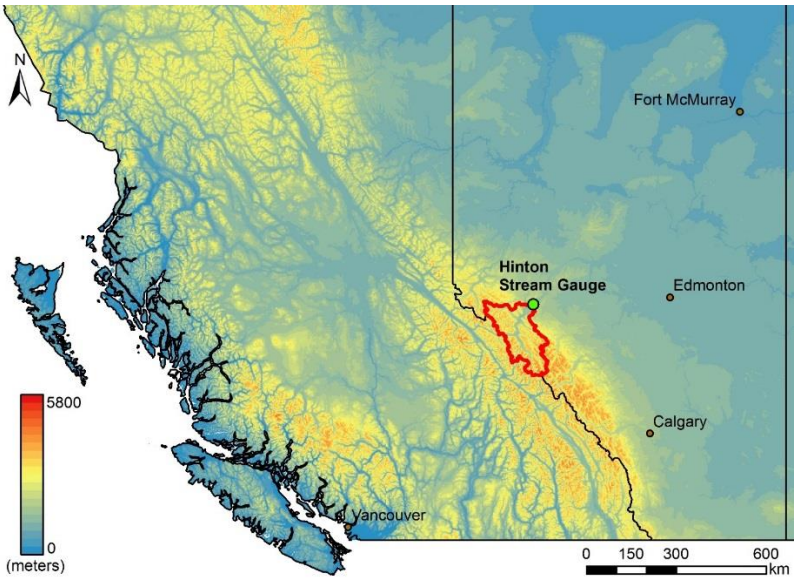

Figure 11: Location of Study Area (outlined in red)

4.3 Data Used

4.3.1 Hydro-Climate Data

River daily discharge data for calibrating and validating the hydrological model were obtained from the Environment Canada hydrometric database (HyDat). Data from the hydrometric station near Hinton, a town on the Athabasca River just downstream from Jasper National Park, were used in this study. The hydrometric stations continuously log river stage and use a stage-flow relationship to calculate discharge.

The ANUSPLIN gridded temperature and precipitation data product (Hutchinson et al., 2009) was used to drive the model over the calibration (2000-2002) and validation (2003-2010) periods. This product utilizes a trivariate thin plate smoothing spline to interpolate temperature or precipitation as measured at Environment Canada weather stations throughout Canada down to a 300 arc second grid (~10 km). Details on the methods and validation of the ANUSPLIN dataset can be found in Hutchinson et al. (2009).

Temperature and precipitation changes associated with future climate scenarios calculated by Dibike et al. (2018) for RCP 8.5 (high emissions scenario) are used to compute future temperature and precipitation data to drive hydrological model projections. Projections from six General Circulation Models (GCMs) from the fifth Climate Model Inter-comparison Project (CMIP5) were examined: CNRM-CM5.1, CanESM2, ACCESS1, INM-CM4, CSIRO-Mk3.6.0, and CCSM4. The spatial resolution of these GCMs varies from 1.25° Longitude by 0.94° Latitude (CCSM4) to 2.8° Longitude by 2.8° Latitude (CanESM2). Therefore, the GCM outputs were statistically downscaled to 10 km resolution using the ANUSPLIN data for the 1951-2010 reference period. Two statistical downscaling techniques were applied for each GCM: Bias-

Correction Spatial Downscaling (BCSD) and Bias Correction/Climate Imprint (BCCI). Basin-averaged temperature and precipitation differences were calculated between the 2041-2070 and 1971-2000 periods. Since 2000-2010 is used as the baseline period in this study, future climate scenarios represent the 2070-2080 period. From these 12 climate change scenarios (6 GCMs x 2 statistical downscaling methods), the scenarios with the highest and lowest annual temperature change were selected for use as 'warm' and 'cool' scenarios in this study. Similarly, the precipitation changes from the wettest and driest scenarios were selected as 'wet' and 'dry' scenarios for this study. These two temperature and two precipitation scenarios were combined into four climate change scenarios representing a range of potential future climates for assessing climate projection uncertainty ('Warm Wet', 'Cool Wet', 'Warm Dry', and 'Cool Dry' scenarios; see Table 4). As temperature and precipitation changes are interdependent, this approach functions as a climate sensitivity analysis.

Temperature Change (°C)				
Scenario	Winter	Spring	Summer	Fall
Cool	4.72	1.66	-1.26	1.86
Warm	6.36	3.57	5.16	4.16

Precipitation Change				
Scenario	Winter	Spring	Summer	Fall
Dry	14.6%	9.2%	-12.5%	7.2%
Wet	32.8%	55.0%	4.7%	27.8%

Table 4: Temperature and precipitation changes for future climate scenarios

4.3.2 Remote Sensing Data

MODIS (Moderate Resolution Imaging Spectroradiometer) imagery was utilized to extract information on snow cover area to be used for the SRM. Multiple MODIS snow cover products are produced by the National Snow and Ice Data Center (NSIDC) including the MOD10 product, providing daily subpixel snow cover fraction at 500-m resolution. This study used the processed snow cover data from Fitzharris and Sirguey (2014) who temporally interpolate the MOD10

snow cover product to fill in cloud covered pixels. The 500-m resolution snow cover data were re-projected into the NAD83(CSRS) 10TM (Forest) cartographic system at 250-m resolution using nearest neighbor sampling. A time series of daily snow cover fraction is created for each pixel. A cubic smoothing spline is used to interpolate snow cover to days where the pixel was obscured by cloud. Frequent cloud cover hinders the use of satellite imagery for measuring snow cover in the winter months. Infrequent imagery makes it difficult to distinguish between the stable seasonal snowpack and shorter-term transitory snow cover. SRM may deal with winter snow cover through assuming complete snow cover during certain months of the year. Alternatively, the seasonal snow cover may be set to zero, and snow depth tracked based on meteorological data. The study utilizes the latter approach.

The Canadian Digital Elevation Model (CDEM), providing 0.75 second (~20 m) resolution elevation data for the Athabasca River Basin, was acquired from the geogratis.gc.ca website.

4.4 Methods

4.4.1 Model Description

Snowmelt Runoff Model (SRM) is a widely used hydrological model for simulating and forecasting daily runoff in mountainous snowmelt dominated catchments. Relatively lighter meteorological data requirements make SRM advantageous in data-scarce mountainous regions, requiring only daily temperature and precipitation, while the utilization of daily remotely sensed snow-cover imagery provides reduced error in snow-cover extent over modelling the snowpack. Several studies have also utilized SRM in examining the hydrological impacts of climate change. The basin is divided into elevation bands (Figure 12) to account for the elevation dependence of the input variables and melt volume is calculated using the

degree-day method. The calculated melt is added with precipitation and transformed into runoff through the recession coefficient, in accordance with the following equation:

$$Q_n = \sum_i (c_{Sin} a_{in} T_{in} SCA_{in} + c_{Rin} P_{in} RCA_{in}) (1 - k(x,y)_n) + Q_{n-1} k(x,y)_n \quad (1)$$

The runoff Q on day n is calculated from the individual contributions of snowmelt, rainfall, and recession from the previous day discharge. The rainfall and snowmelt contributions are summed over each elevation zone i. Snowmelt for each zone is calculated using the mean daily temperature over the zone, T, the Degree Day Factor (DDF), a, and multiplying by the snow covered area, SCA to obtain melt volume. Rainfall runoff is calculated using the rainfall depth, P and multiplying by the rainfall contributing area RCA. A calibrated threshold value (the critical temperature) is used to differentiate rain from snow. If the zonal temperature is below the critical temperature, precipitation is determined to fall as snow and does not contribute immediately to runoff. Accumulated snow due to precipitation is tracked until positive temperatures release the stored water content to contribute to runoff. The runoff coefficients c_S and c_R account for losses due to evaporation and sublimation. The recession coefficient $k(x,y)$, transforms the daily influx of water into runoff. The recession coefficient is a function of the calibrated parameters x and y. A complete description of the model can be found in Martinec et al. (2008).

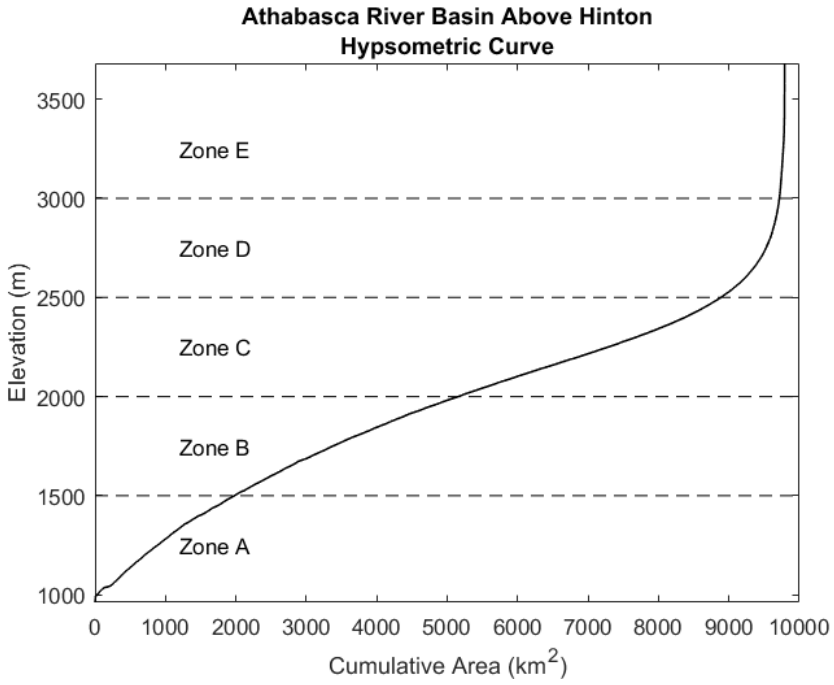

Figure 12: Hypsometric curve for study area with elevation bands

Melt depth is calculated using a degree-day model in place of a more data-intensive energy balance model, as degree day models can obtain accurate results despite their simplicity (Hock, 2003). Multiple approaches to the DDF were evaluated in Chapter 3. As glacial ice has a higher DDF than snow due to its lower albedo, the use of a separate DDF for snow versus glacial ice proved essential in capturing interannual variability in flow conditions. The DDF varies seasonally due to changing melt conditions, with increasing solar radiation and decreasing albedo contributing to increased melt and a higher DDF as the melt season progresses. Chapter 3 evaluated the calibration on monthly DDF values typical of many SRM studies, as well as the approach of sinusoidally varying the DDF between calibrated minimum and maximum values occurring on the solstices. The sinusoidal variation of the DDF has been shown by Anderson (2006) and in Chapter 3 to provide similar quality results to the monthly approach while having

fewer parameters to calibrate. The sinusoidal approach with separate glacier DDF was selected for use in this study.

4.4.2 Model Calibration

The SRM was calibrated using the years 2000-2002 and subsequently validated over the years 2003-2010. Model calibration and uncertainty assessment was carried out using the Metropolis algorithm, a Monte Carlo Markov Chain (MCMC) method. Parameters are limited to a range of plausible values and are iteratively adjusted as part of a random walk through the parameter space. This calibration and uncertainty analysis method has previously been applied to SRM by Panday et al (2014). The acceptance of new parameter sets along this random walk is based on the cost function, a measure of model fit. The cost function used was the Nash Sutcliffe Efficiency (NSE), a common measure of model fit in hydrological modelling. By rejecting parameter sets with reduced model fit with a probability based on the magnitude of the reduction, the random walk will eventually converge on an optimum parameter set. The metropolis algorithm developed by Metropolis et al. (1953) introduced several techniques used to increase optimization speed and ensure the global optimum is found rather than local optima. The final product is a collection of accepted parameter values which can be used to assess parameter uncertainty, with the best result (as measured by the cost function) serving as the 'definitive' solution.

4.4.3 Simulation of Future Climate

Climate change impacts are investigated by applying the calculated change in temperature and percentage change in precipitation (Table 4) corresponding to each of the four scenarios to the baseline climate (2000-2010) data. The model is run using the adjusted variables and compared

to the model results for the base case climate. Snow cover is adjusted to account for reduced accumulation in winter and more rapid melt under warmer temperatures. While use of remotely sensed imagery in SRM was advantageous for improved accuracy in snow cover for modelling historical snowmelt, this advantage is reduced for climate change projections where changes in snow cover area must be modelled. The methodology for deriving snow cover under a future climate is briefly outlined here, a more detailed description is available in Martinec et al., (2008). Conventional depletion curves for each elevation band are produced by averaging the snow cover fraction across all pixels in the elevation band for each day. These curves represent the pattern of snow cover depletion for the present climate. Snowfall occurring during the melt season may be reduced or no longer occur under a warmer climate. As these curves are intended to be extrapolated for future climate, snowfall events occurring after April 1st are removed before creating this relationship to not include snow cover increases which may not occur in the future climate. Snowfall after April 1st is instead accounted for using meteorological data. If the temperature is below the critical temperature, precipitation is determined to fall as snow, and is stored by the model until released through snow melt.

To project snow cover into the future, a relationship between snow cover fraction and cumulative melt depth is established using historical data. For each historical year, cumulative melt depth is calculated for each day starting from April 1st using positive degree days and the calibrated DDF. Since melt season SCA increases were removed in the previous step, cumulative melt associated with melt season snowfall events is removed from the cumulative melt calculation. The cumulative melt depth for each day is then related to the observed SCA on that day, creating the relationship which is utilized for projecting future SCA. Using the temperature

and precipitation data for the future climate, cumulative melt depth is calculated using the same methodology as before. SCA is then calculated for the future climate using the established melt depth – SCA relationship. The increase in calculated melt depth resulting for projected warmer temperature will result in a corresponding more rapid depletion in SCA using this method.

Decreases in winter accumulation are accounted for by first calculating the SWE on April 1st. The April 1st SWE for each zone is estimated using precipitation and temperature data over the winter months (October – March). As with during the melt season, if the zonal temperature is below the critical temperature, precipitation is determined to fall as snow and is added to snow storage for that zone. Similarly, melt is calculated from positive degree days and subtracted from this snow storage. At the end of the winter period (April 1st), a final snow storage SWE is obtained. This April 1st SWE is calculated using both the historical and future temperature and precipitation data. The difference between the historical and future climate April 1st SWE is then added to the future climate cumulative melt depth using in projecting the new SCA. Thus if April 1st SWE is determined to have declined, the initial cumulative melt depth is set equal to that decline, resulting in a reduction in SCA under the future climate. Conversely, if SWE is calculated to have increased at the end of the winter season, the cumulative melt depth must equal the increase in SWE before SCA can decline.

The standard version of SRM does not include a glacial component, with glacial ice treated identically to snow cover. This study includes a separate DDF for glacial ice as the lower albedo of ice results in an increased melt rate. The minimum observed SCA over the historical period (2000-2010) was used to estimate glacier area. Glacier dynamics were not modelled in this

study; instead, estimated glacier declines from Clarke et al. (2015) were utilized. Clarke et al. (2015) modelled changes in glacier volume and area across BC and Alberta over the 21st century utilizing climate projections from six GCM's. The 200-m resolution glacier area product produced by Clarke et al. (2015) was applied in adjusting glacier area for the Upper Athabasca watershed. Glacierized fraction was calculated for each elevation band in the study basin for historical (2000-2009) and future (2070-2080) time periods. Glacier area estimates in our study differ from Clarke et al. (2015), thus a percentage reduction in glacier area for each elevation band was calculated and applied to the glacier areas used in SRM (Table 5). Seasonal snow may still be present in previously glaciated areas, therefore formally glaciated areas were converted to snow (applying snow DDF in place of glacier DDF) rather than removed from the melt calculation altogether. Percentage area change for each zone was averaged over all six climate change scenarios for use in this study.

Elevation Band (m)	Glacier Area (km^2)	Glacier Area Change (%)
960-1500	0	N/A
1500-2000	1	-81
2000-2500	31	-67
2500-3000	116	-58
3000-3740	33	-20

Table 5: Glacier area (as calculated from MODIS SCA minimum) and projected percentage change in glacier area for each elevation band

4.5 Results

4.5.1 Snow Cover Area

Increased temperatures generally resulted in decreased SCA under all future climate scenarios, though the extent of the decrease is dependent on the scenario, elevation zone, and time of year (Figure 13, Figure 14). In general, the greatest decreases in SCA occurred in the lower

elevation bands. Higher elevation bands experienced lower reductions in SCA, or in some cases increases in SCA (for wet/cool scenarios) depending on whether increased snowfall compensated for increased melt. For example, the 960-1500 m band experienced a 40-70% reduction in SCA at the start of the melt season (April 1st) due to reduced winter snowfall, whereas the 3000-3740 m elevation band experienced less than a 10% decline.

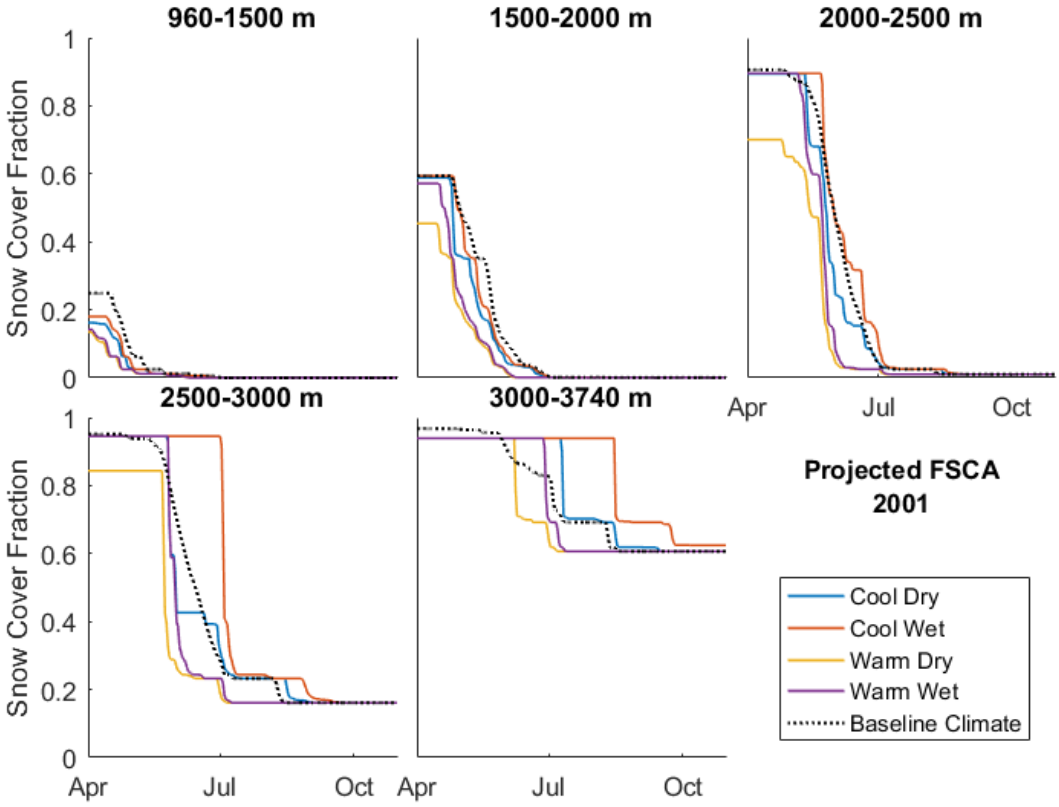

Figure 13: Snow cover depletion curves for each elevation zone and climate scenario for 2001.

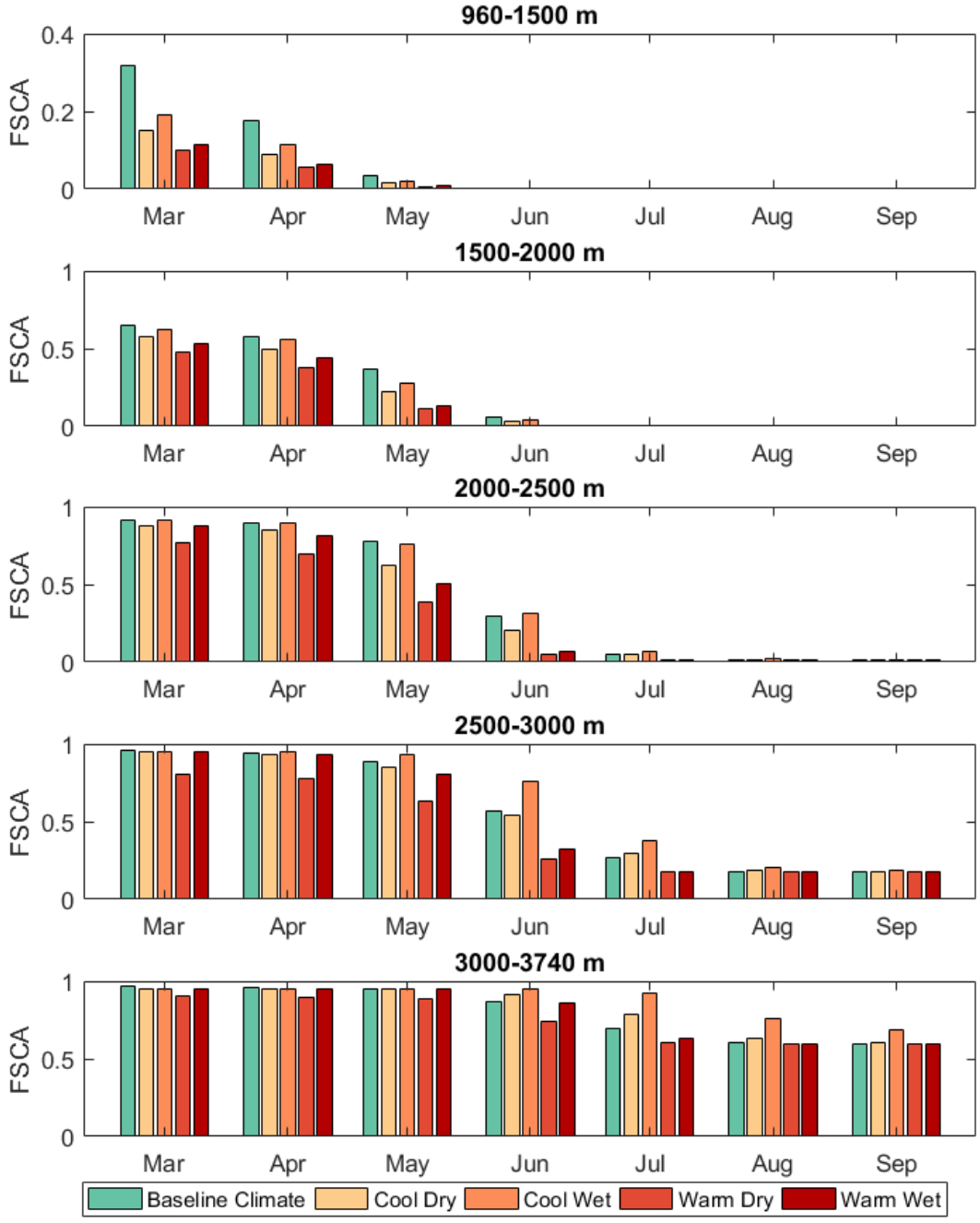

Figure 14: Snow cover fraction projections for 2070-2080 for each elevation band

In the lower elevation zones, May experiences the largest percentage decline in SCA of any month. The month experiencing the largest percentage decline in SCA shifts later in the year to June or July at higher elevation zones. Little or no decline occurs after August, as the methodology for calculating snow cover under the future climate does not allow SCA to drop below the minimum observed SCA for that zone. With the SCA minimum typically occurring in August or September, no further decline is possible. While the largest percentage change in SCA occurs between May and July (depending on elevation zone and climate change scenario), the largest absolute change in SCA generally occurs in April or May due to more extensive snow cover in these months.

The largest declines in SCA occurred under the 'Warm Dry' scenario, closely followed by the 'Warm Wet' Scenario. SCA was highest under the 'Cool Wet' scenario, with increases in SCA at higher elevations due to increased precipitation. These results demonstrate temperature being a larger factor for SCA decline than precipitation over the range of GCM outputs considered, as the 'Warm Wet' scenario demonstrates a larger decline in SCA than the 'Cool Dry' scenario.

4.5.2 Runoff

The calibrated SRM is run using the modified SCA corresponding to each of the four climate scenarios. The results show that mean annual discharge (MAD) declined under the 'Cool Dry' scenario, whereas increased MAD was projected for all other climate change scenarios. Changes in MAD ranged from -23.7 m^3/s (-14.9%) for the 'Cool Dry' scenario to +35.2 m^3/s (+22.1%) for the 'Warm Wet' scenario, deviating from the baseline climate MAD of 159.2 m^3/s. Larger declines were experienced by the 'Cool' scenarios relative to the 'Warm' scenarios due to lower glacial melt associated with lower temperatures. The use of a set decline in glacier

area for all four climate change scenarios is a source of error in this result, as in reality the greater reduction in glacier area under the 'Warm' scenarios may overpower the increase in melt.

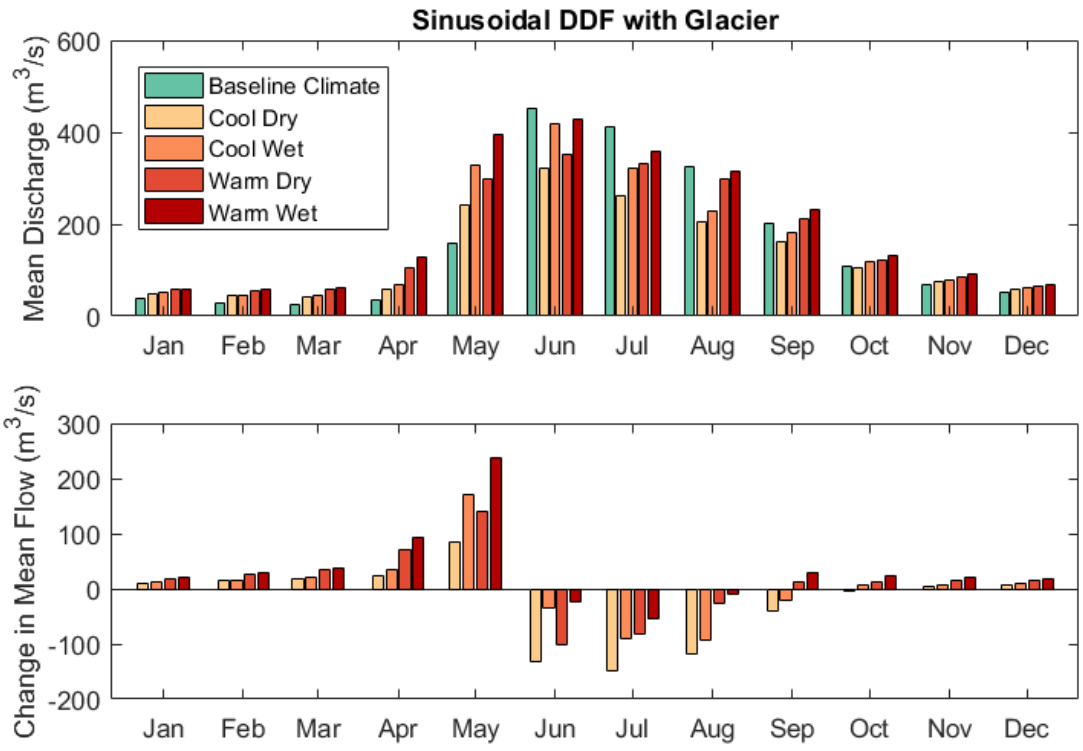

Figure 15: Mean monthly discharge for baseline (2000-2010) climate and four 2070-2080 climate change scenarios (top), and difference in monthly discharge between the future and baseline climate (bottom)

Model results show the shift to an earlier spring freshet (Figure 15) consistent with observed trends (Rood et al., 2008) and the expected consequence of a warmer climate (Barnett et al., 2005). Increases in runoff occur in the months October through May resulting from warmer temperatures and the consequential increase in winter rainfall and snowmelt. May experiences the largest increase in runoff of any month regardless of climate change scenario, ranging from an increase of 85 m^3/s (Cool Dry) to 237 m^3/s (Warm Wet). The earlier depletion of the seasonal snowpack produces lower flows for all scenarios in June through August, and lower flows for

the Cool Wet and Cool Dry Scenarios in September. The Warm Dry and Warm Wet scenarios display higher runoff than the Cool scenarios in all months except May and June, where the Cool Wet and Warm Wet scenarios display higher runoff.

Historical runoff trends for the Athabasca River near Jasper show statistically significant decreases in flow for the months of July, August, and September over the period of 1914-2005 (Rood et al. 2008). My results also show similar seasonal pattern of reductions in modelled flow in June, July, and August, with little change in September flow. The projected decline in June flow, a month where no significant decline has been observed historically, shows the progressively earlier depletion of the snowpack. Increased melt runoff from glaciers offsets earlier depletion of snow cover, but glacierized area is also reduced. The historical decreasing trend in September runoff contrasts the absence of change in the projected flow. Snow cover over the baseline period (2000-2010) reached its minimum by August, and the methodology for simulating future SCA precludes modelled SCA below the observed minimum. This limitation will result in overestimation of flows in late summer when SCA could be expected to decline below its historically observed minimum. The accuracy of SCA projections and the use of a set change in glacier area across all climate change scenarios lend additional uncertainty. Interpolated precipitation has greater uncertainty at higher elevations due to the rarity of high elevation weather stations, which will contribute to greater uncertainty to SCA projections in these elevation bands.

The modelled increase in MAD for most climate scenarios is not consistent with the observed historical decreasing trend (Bawden et al., 2014). However, the historical decreasing trend may not continue in the future, and in this regard, my results are consistent with modelling studies

such as Eum et al. (2017) and Toth et al. (2006) that projected increased MAD, increased spring flows and decreased summer flows. The percentage change in annual and seasonal flows presented for Hinton in Eum et al. (2017) lie within the range of flows projected using the four climate change scenarios in this thesis. For example, Eum et al. (2017) project an 88% increase in spring flows, within the 59% to 171% range obtained here. These results contrast to those presented in Shrestha et al. (2017) who projected declining Spring runoff due to a reduced Winter snowpack and increasing Summer runoff due to increased precipitation. The climate change scenario for the Athabasca headwaters regions (above the Hinton, Alberta) used in Shrestha et al. (2017) showed a decline in mean annual temperature in contrast to increasing temperature indicated in other studies, which may account for this discrepancy in runoff projections.

4.5.3 Parameter Uncertainty

The effect of parameter uncertainty on runoff was examined using the parameter sets generated from MCMC simulations. The change in runoff is calculated for each parameter set by simulating both the present and future runoff with the same parameter set and taking the difference between the two. Results show the relative impacts of the different climate scenarios are consistent when accounting for parameter uncertainty, with the Warm Wet scenario generating the largest increase in MAD and the Cool Dry scenario generating the largest decrease in MAD for all parameter sets (Figure 16). The Warm Dry future scenario produces higher MAD than the Cool Wet scenario for 97.3% of parameter sets. Mean annual discharge declines in 99% of parameter sets for the Cool Dry scenario, while all other climate change scenarios experience increases in MAD for >99% of parameter sets. There is a negative

correlation between calibration period model fit and projected future climate MAD (Pearson R = 0.35–0.59, depending on climate change scenario). The optimal parameter set (the parameter set with the best model fit) displays much lower MAD under a future climate than the median MAD of all parameter sets for each climate change scenario.

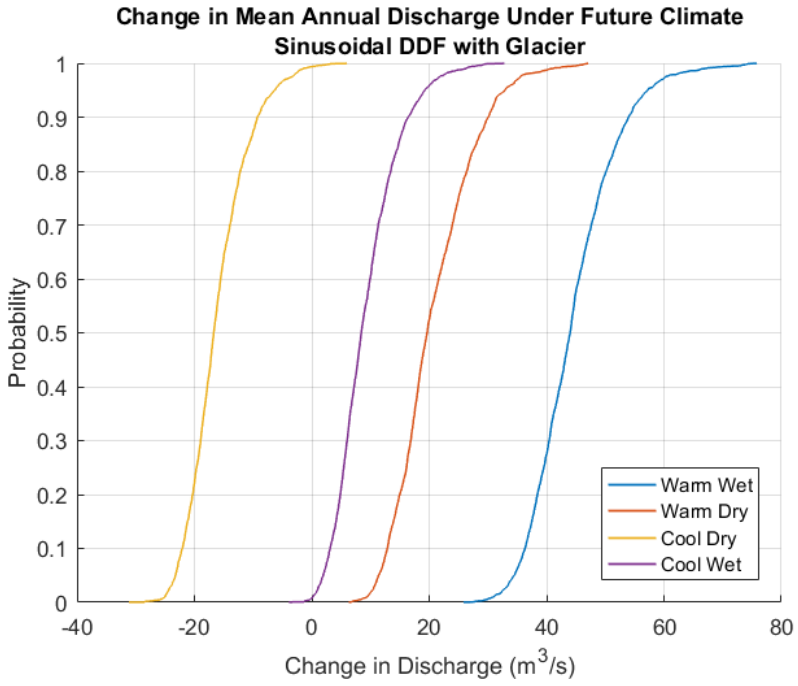

Figure 16: Cumulative probability density function for change in Mean Annual Discharge between baseline climate and the four future climate change scenarios for all parameter sets

May consistently shows the greatest increase in discharge of any month (With May having the largest increase in discharge for all simulation in the Warm Wet and Cool Wet scenarios, and for more than 98% of simulations for the other scenarios). April has the largest or (more often) second largest increase in discharge of any month in 99% of simulations. June and July experience the largest decreases in flow. Earlier depletion of the snowpack leads to earlier reduction of summer flows, thus the warmer climate scenarios experience decreased flows earlier in the year with July experiencing the largest decrease in 77% of simulations under the

Cool Wet scenario and June experiencing the largest decrease in 61% of simulations under the Warm Dry scenario.

Correlation analysis shows runoff volume over the winter half of the year (October – March) is strongly correlated with the winter DDF, the Pearson R correlations ranging from 0.93 to 0.96, depending on climate change scenario. As little melt occurred over the winter months historically, the winter DDF does not affect model fit. With warming winter temperatures under climate change, the winter DDF gains a much larger impact on model results. Prescribing a sinusoidal pattern to temporal variation in the DDF constrains the winter DDF to a limited range of values. The winter DDF must be realistically constrained during the calibration process for climate change studies, as its lack of impact on model fit will result in a poorly defined parameter which will contribute substantial uncertainty to climate change projections.

4.6 Conclusion

The impacts of climate change on runoff for the Athabasca River at Hinton were simulated using the Snowmelt Runoff Model. Four climate change scenarios were examined to capture uncertainty in climate change projections. Snow cover area is projected to decline, with the largest declines occurring at lower elevations. Results show a substantial increase in projected runoff for the month of May and a smaller but still notable increase in April. Increased runoff for October through March is small relative to the increases in April and May, but large relative to the historically low winter flows over these months. In addition to the largest increases in flow, April and May experience the largest declines in snow cover area. The shift towards an earlier freshet and corresponding earlier depletion of the spring snowpack result in lower summer flows, with June, July, and August experiencing decreases. These trends were robust

when accounting for parameter uncertainty, and consistent with observed historical trends and other modelling studies. The Snowmelt Runoff Model provides a relatively simple tool for assessing climate change impacts on river flow.

References

Adam, J. C., Hamlet, A. F., & Lettenmaier, D. P. (2009). Implications of global climate change for snowmelt hydrology in the twenty-first century. *Hydrological Processes*, *23*(1), 962–972.

Anderson, E. (2006). Snow Accumulation and Ablation Model–SNOW-17. *Online Documentation*, 1–61.

Barnett, T. P., Adam, J. C., & Lettenmaier, D. P. (2005). Potential impacts of a warming climate on water availability in snow-dominated regions. *Nature*, *438*, 303–309.

Bawden, A. J., Linton, H. C., Burn, D. H., & Prowse, T. D. (2014). A spatiotemporal analysis of hydrological trends and variability in the Athabasca River region, Canada. *Journal of Hydrology*, *509*, 333–342.

Clarke, G. K. C., Jarosch, A. H., Anslow, F. S., Radić, V., & Menounos, B. (2015). Projected deglaciation of western Canada in the twenty-first century. *Nature Geoscience*, *8*(5), 372–377.

Dibike, Y., Eum, H. Il, & Prowse, T. (2018). Modelling the Athabasca watershed snow response to a changing climate. *Journal of Hydrology: Regional Studies*, *15*, 134–148.

Eum, H., Dibike, Y., & Prowse, T. (2017). Climate-Induced Alteration of Hydrologic Indicators in the Athabasca River Climate-induced alteration of hydrologic indicators in the Athabasca River Basin , Alberta , Canada. *Journal of Hydrology*, *544*(December 2017), 327–342.

Fitzharris B. & Sirguey P. (2014). Building a Platform for Snowmelt Runoff Modelling in the Athabasca River Basin, *Unpublished Report*

Hock, R. (2003). Temperature index melt modelling in mountain areas. *Journal of Hydrology*, *282*(1–4), 104–115.

Hutchinson, M. F., McKenney, D. W., Lawrence, K., Pedlar, J. H., Hopkinson, R. F., Milewska, E., & Papadapol, P. (2009). Development and Testing of Canada-Wide Interpolated Spatial Models of Daily Minimum – Maximum Temperature and Precipitation for 1961 – 2003, 725–741.

Ma, Y., Huang, Y., Chen, X., Li, Y., & Bao, A. (2013). Modelling snowmelt runoff under climate change scenarios in an ungauged mountainous watershed, Northwest China. *Mathematical Problems in Engineering*.

Martinec, J., Rango, a, & Roberts, R. (2008). Snowmelt runoff model (SRM) user's manual. *Agricultural Experiment Station Special Report 100*.

Metropolis, N., Rosenbluth, A. W., Rosenbluth, M. N., Teller, A. H., & Teller, E. (1953). Equation of State Calculations by Fast Computing Machines, *1087*.

Nolin, A. W., Phillippe, J., Jefferson, A., & Lewis, S. L. (2010). Present-day and future contributions of glacier runoff to summertime flows in a Pacific Northwest watershed: Implications for water resources. *Water Resources Research*, *46*(12), 1–14.

O'Neil, H. C. L., Prowse, T. D., Bonsal, B. R., Dibike, Y. B. (2016a) Spatial and temporal characteristics in streamflow-related hydroclimatic variables over western Canada. Part 1: 1950–2010. *Hydrology Research*, *48* (4), 915–931.

O'Neil, H. C. L., Prowse, T. D., Bonsal, B. R., Dibike, Y. B. (2016b) Spatial and temporal characteristics in streamflow-related hydroclimatic variables over western Canada. Part 2: future projecctions. *Hydrology Research*, *48* (4), 932–944.

Rango, A., Martinec, J., & Roberts, R. (2008). Relative importance of glacier contributions to water supply in a changing climate. *World Resource Review*, *20*(3), 487–503.

Rood, S. B., Pan, J., Gill, K. M., Franks, C. G., Samuelson, G. M., & Shepherd, A. (2008). Declining summer flows of Rocky Mountain rivers: Changing seasonal hydrology and probable impacts on floodplain forests. *Journal of Hydrology*, *349*, 397–410.

Schindler, D. W., & Donahue, W. F. (2006). An impending water crisis in Canada's western prairie provinces. *Proceedings of the National Academy of Sciences of the United States of America*, *103*(19), 7210–6.

Stahl, K., & Moore, R. D. (2006). Influence of watershed glacier coverage on summer streamflow in British Columbia, Canada. *Water Resources Research*, *42*(6), 2–6.

Tahir, A. A., Chevallier, P., Arnaud, Y., Neppel, L., & Ahmad, B. (2011). Modeling snowmelt-runoff under climate scenarios in the Hunza River basin, Karakoram Range, Northern Pakistan. *Journal of Hydrology*, *409*(1–2), 104–117.

Toth, B., Pietroniro, A., Conly, F. M., & Kouwen, N. (2006). Modelling climate change impacts in the Peace and Athabasca catchment and delta : I — hydrological model application, *4214*, 4197–4214.

5 Chapter 5: Conclusions

This thesis modelled climate change impacts on runoff for the Upper Athabasca River Basin (UARB) in Alberta, Canada. The Snowmelt Runoff Model (SRM), a simple conceptual hydrological model intended for snowmelt dominated catchments such as the UARB, was utilized in achieving the objectives of this study. The primary objectives of this thesis were to:

(1) Assess the ability of the Snowmelt Runoff Model to accurately capture runoff for the Upper Athabasca River
(2) Utilize SRM in assessing the effects of climate change on the seasonal distribution of runoff for the Upper Athabasca River

Chapter 2 presented a literature review of the historical development of melt modelling and SRM, and the strengths and weaknesses of SRM. Chapter 3 addressed objective (1), assessing the performance of SRM in simulating historical flows for the UARB as well as comparing multiple approaches to handling the melt calculation. The results of Chapter 3 informed the application of SRM in addressing objective (2) in Chapter 4. Projected changes in temperature and precipitation for four climate change scenarios were examined using the calibrated hydrological model to project runoff for the 2070-2080 period relative to the baseline 2000-2010 period.

SRM was calibrated and validated using historical flow data from the Athabasca River at Hinton hydrometric station for the years 2000-2010. Ensuring the model performs well over a range of years with varying meteorological and hydrological conditions is important for model applicability outside of the calibration period. The absence of field measurements from the study basin, along with the tenuous relationship between model parameters and actual

hydrological processes (Ferguson, 1999), meant model parameters were determined solely through calibration within set limits of physically plausible values. Given the importance of the Degree Day Factor (DDF) in determining runoff volume in snowmelt dominated basins, multiple approaches to handling this parameter and its spatial and temporal variability were examined. The Monte Carlo Markov Chain method was utilized for model calibration, given its relatively quick runtime and built in assessment of parameter uncertainty. Calibration was performed over the 2000-2002 period, years which presented sufficient variability for the model to perform well over the validation period (2003-2010).

Variations on the DDF parameter tested included calibrating individual monthly values versus assuming a sinusoidal pattern in the temporal variation of the parameter. Given the difference in DDF values between snow and exposed glacial ice, the inclusions of a separate glacier DDF was also tested. The sinusoidal DDF was found to perform on par with the monthly DDF, accurately capturing the seasonal variation in DDF while requiring fewer parameters to calibrate. The sinusoidal DDF pattern also constrained winter DDF values, which had limited impact on model results over the historical period but had a larger impact on runoff when applied to a warmer climate. Model results showed the inclusion of the glacier DDF resulted in a notable increase in model fit and was vital in capturing interannual variability in melt conditions. The glacial DDF approach performed similarly to the traditional SRM approach of varying the DDF by elevation band, indicating the higher DDF for glacial ice can account for much of the elevational dependence of the DDF. Overall model performance was deemed satisfactory for application in hydrological projections with the glacier component included, with average Nash Sutcliffe Efficiencies of 0.94 and 0.87 over the calibration and validation

periods, respectively. Some persistent sources of model error were present, including underestimation of June and July runoff peaks. This early summer flow underestimation may be the result of the underestimation of snow cover area when snow cover is patchy by the MODIS product noted by previous studies (Déry et al., 2005; Kult et al., 2014). The use of higher resolution imagery to correct for snow cover underestimation should be included in future SRM applications, as suggested by Kult et al. (2014). Model performance also appeared to be limited by the simplistic representation of runoff routing in SRM.

The sinusoidal DDF with glacier component approach was selected for performing runoff projections under a changed climate. Four climate scenarios for the 2070-2080 period were examined to account for uncertainty in climate change projections. The month of May experienced a substantial increase in runoff across all four scenarios, while June and July experienced decreases, consistent with the historical trend of an earlier freshet and decreasing summer flow. Snow cover area experienced a corresponding large decrease in May, with the largest decreases occurring at low elevation. Smaller runoff increases occurred over the winter months, though these increases represented a substantial percentage change due to the historically low runoff during these months. SRM parameter uncertainty was not found to substantially alter model results. While this study examined the effects of parameter uncertainty as determined during calibration, it did not account for the temporal evolution of parameter values under a changed climate. Farther investigation on the effects of varying climate conditions on parameter values such as the DDF, runoff coefficients, and recession coefficients would be beneficial in ensuring the robustness of hydrological projections.

Future work should utilize higher resolution snow cover imagery to address snow cover underestimation by MODIS. Inclusion of a simple glacier model would benefit application in regions where glacial melt is significant. Whereas this thesis utilized a set reduction in glacier area for all climate change scenarios, glacier area will depend on climate and should be modelled for each scenario. While the use of remotely sensed snow cover imagery provides increased accuracy over simulating the snowpack for historical data, this advantage is reduced for climate change projections if snow cover depletion patterns differ under the changed climate. A more detailed investigation of interannual snow conditions or examining changes in snow cover depletion patterns with a more detailed physics-based model could be used to estimate the error associated with the SRM snow cover projection methodology. This methodology could be expected to be more advantageous for short term forecast, where snow conditions are more likely to be similar to the calibration period. Many studies have examined the utility of SRM as a short-term forecasting tool, and future work could examine the real time assimilation of satellite imagery for runoff forecasting.

References

Déry, S. J., Salomonson, V. V., Stieglitz, M., Hall, D. K., & Appel, I. (2005). An approach to using snow areal depletion curves inferred from MODIS and its application to land surface modelling in Alaska. *Hydrological Processes*, *19*(14), 2755–2774.

Ferguson, R. I. (1999). Snowmelt runoff models. *Progress in Physical Geography*, *23*, 205–227.

Kult, J., Choi, W., & Choi, J. (2014). Sensitivity of the Snowmelt Runoff Model to snow covered area and temperature inputs. *Applied Geography*, *55*, 30–38